

NUCLEAR MODELS

At this point it is tempting to try to extend the ideas of the previous chapter to heavier nuclei. Unfortunately, we run into several fundamental difficulties when we do. One difficulty arises from the mathematics of solving the many-body problem. If we again assume an oversimplified form for the nuclear potential, such as a square well or an harmonic oscillator, we could in principle write down a set of coupled equations describing the mutual interactions of the A nucleons. These equations cannot be solved analytically, but instead must be attacked using numerical methods. A second difficulty has to do with the nature of the nuclear force itself. There is evidence to suggest that the nucleons interact not only through mutual two-body forces, but through three-body forces as well. That is, the force on nucleon 1 not only depends on the individual positions of nucleons 2 and 3, it contains an *additional* contribution that arises from the correlation of the positions of nucleons 2 and 3. Such forces have no classical analog.

In principle it is possible to do additional scattering experiments in the three-body system to try (in analogy with the two-body studies described in Chapter 4) to extract some parameters that describe the three-body forces. However, we quickly reach a point at which such a microscopic approach obscures, rather than illuminates, the essential physics of the nucleus. It is somewhat like trying to obtain a microscopic description of the properties of a gas by studying the interactions of its atoms and then trying to solve the dynamical equations that describe the interatomic forces. Most of the physical insight into the properties of a gas comes from a few general parameters such as pressure and temperature, rather than from a detailed microscopic theory.

We therefore adopt the following approach for nuclei. We choose a deliberately oversimplified theory, but one that is mathematically tractable and rich in physical insight. If that theory is fairly successful in accounting for at least a few nuclear properties, we can then improve it by adding additional terms. Through such operations we construct a *nuclear model*, a simplified view of nuclear structure that still contains the essentials of nuclear physics. A successful model must satisfy two criteria: (1) it must reasonably well account for previously measured nuclear properties, and (2) it must predict additional properties that can be measured in new experiments. This system of modeling complex processes is a common one in many areas of science; biochemists model the complex processes such as occur in the replication of genes, and atmospheric

scientists model the complex dynamics of air and water currents that affect climate.

5.1 THE SHELL MODEL

Atomic theory based on the shell model has provided remarkable clarification of the complicated details of atomic structure. Nuclear physicists therefore attempted to use a similar theory to attack the problem of nuclear structure, in the hope of similar success in clarifying the properties of nuclei. In the atomic shell model, we fill the shells with electrons in order of increasing energy, consistent with the requirement of the Pauli principle. When we do so, we obtain an inert core of filled shells and some number of valence electrons; the model then assumes that atomic properties are determined primarily by the valence electrons. When we compare some measured properties of atomic systems with the predictions of the model, we find remarkable agreement. In particular, we see regular and smooth variations of atomic properties *within* a subshell, but rather sudden and dramatic changes in the properties when we fill one subshell and enter the next. Figure 5.1 shows the effects of a change in subshell on the ionic radius and ionization energy of the elements.

When we try to carry this model over to the nuclear realm, we immediately encounter several objections. In the atomic case, the potential is supplied by the Coulomb field of the nucleus; the subshells ("orbits") are established by an external agent. We can solve the Schrödinger equation for this potential and calculate the energies of the subshells into which electrons can then be placed. In the nucleus, there is no such external agent; the nucleons move in a potential that they themselves create.

Another appealing aspect of atomic shell theory is the existence of spatial orbits. It is often very useful to describe atomic properties in terms of spatial orbits of the electrons. The electrons can move in those orbits relatively free of collisions with other electrons. Nucleons have a relatively large diameter compared with the size of the nucleus. How can we regard the nucleons as moving in well defined orbits when a single nucleon can make many collisions during each orbit?

First let's examine the experimental evidence that supports the existence of nuclear shells. Figure 5.2 shows measured proton and neutron separation energies, plotted as deviations from the predictions of the semiempirical mass formula, Equation 3.28. (The gross changes in nuclear binding are removed by plotting the data in this form, allowing the shell effects to become more apparent.) The similarity with Figure 5.1 is striking—the separation energy, like the atomic ionization energy, increases gradually with N or Z except for a few sharp drops that occur at the same neutron and proton numbers. We are led to guess that the sharp discontinuities in the separation energy correspond (as in the atomic case) to the filling of major shells. Figure 5.3 shows some additional evidence from a variety of experiments; the sudden and discontinuous behavior occurs at the same proton or neutron numbers as in the case of the separation energies. These so-called "magic numbers" (Z or $N = 2, 8, 20, 28, 50, 82,$ and 126) represent the effects of filled major shells, and any successful theory must be able to account for the existence of shell closures at those occupation numbers.

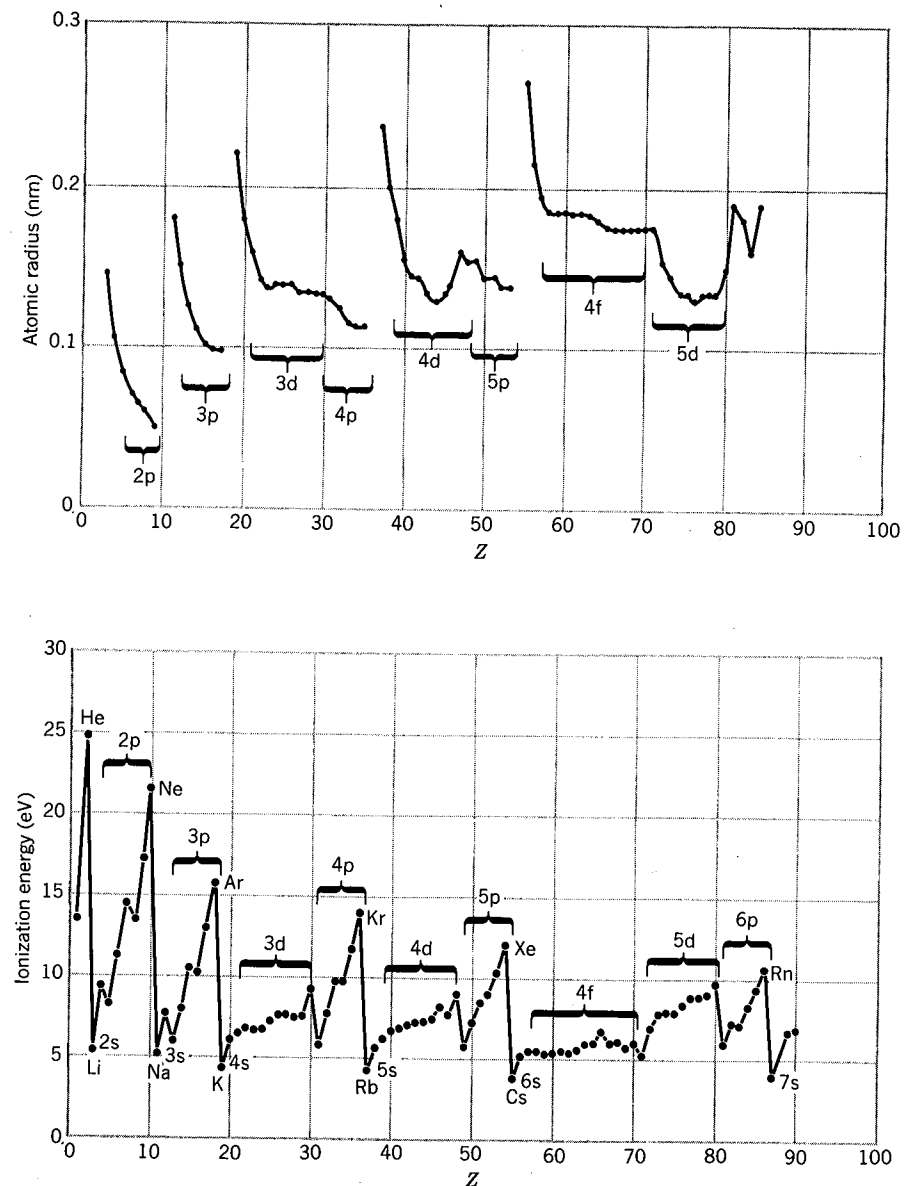


Figure 5.1 Atomic radius (top) and ionization energy (bottom) of the elements. The smooth variations in these properties correspond to the gradual filling of an atomic shell, and the sudden jumps show transitions to the next shell.

The question of the existence of a nuclear potential is dealt with by the fundamental assumption of the shell model: the motion of a single nucleon is governed by a potential caused by all of the other nucleons. If we treat each individual nucleon in this way, then we can allow the nucleons in turn to occupy the energy levels of a series of subshells.

The existence of definite spatial orbits depends on the Pauli principle. Consider in a heavy nucleus a collision between two nucleons in a state near the very

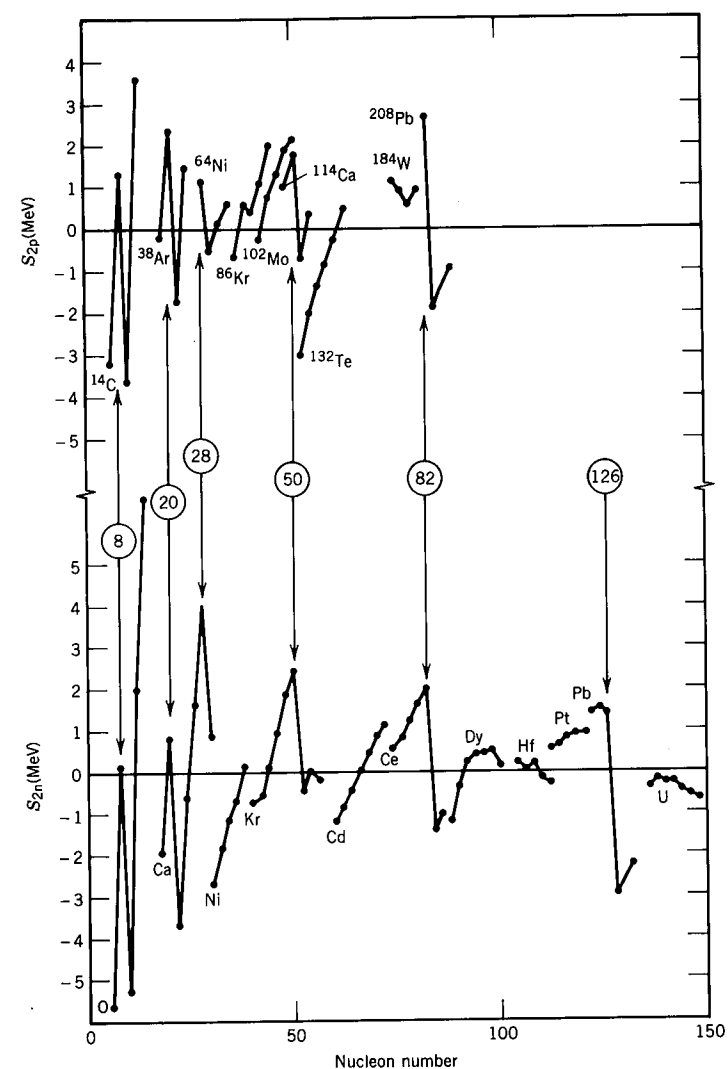


Figure 5.2 (Top) Two-proton separation energies of sequences of isotones (constant N). The lowest Z member of each sequence is noted. (Bottom) Two-neutron separation energies of sequences of isotopes. The sudden changes at the indicated "magic numbers" are apparent. The data plotted are differences between the measured values and the predictions of the semiempirical mass formula. Measured values are from the 1977 atomic mass tables (A. H. Wapstra and K. Bos, *Atomic Data and Nuclear Data Tables* **19**, 215 (1977)).

bottom of the potential well. When the nucleons collide they will transfer energy to one another, but if all of the energy levels are filled up to the level of the valence nucleons, there is no way for one of the nucleons to gain energy except to move up to the valence level. The other levels near the original level are filled and cannot accept an additional nucleon. Such a transfer, from a low-lying level to the valence band, requires more energy than the nucleons are likely to transfer in

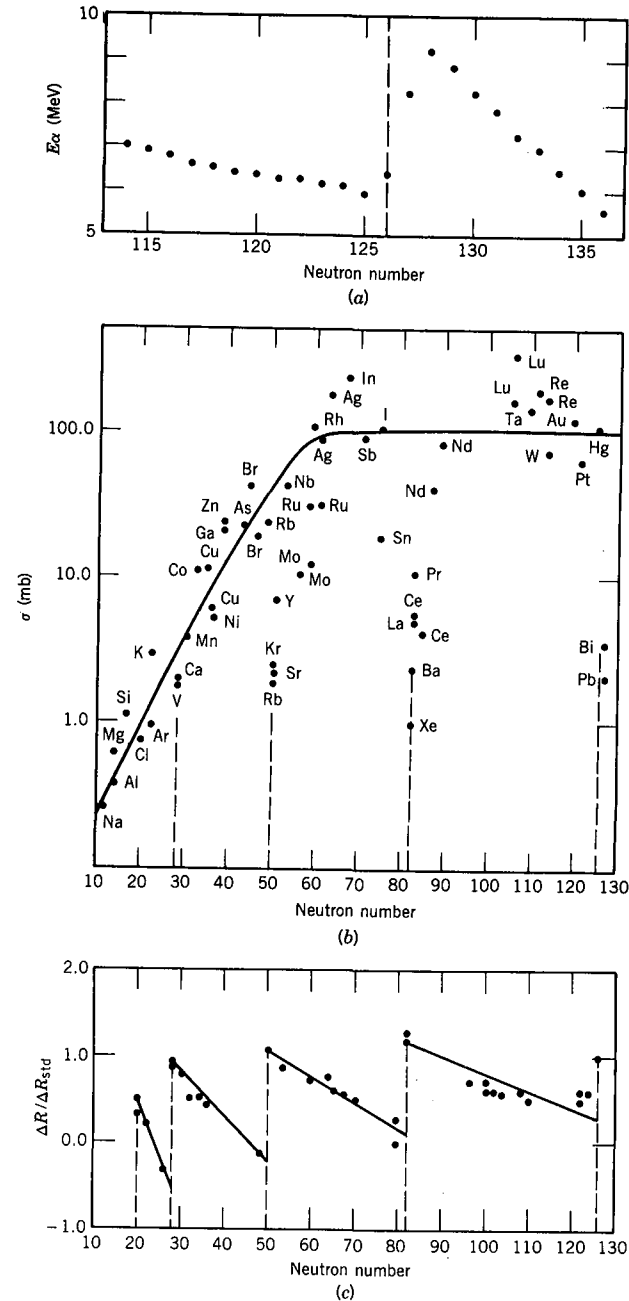


Figure 5.3 Additional evidence for nuclear shell structure. (a) Energies of α particles emitted by isotopes of Rn. Note the sudden increase when the *daughter* has $N = 126$ (i.e., when the parent has $N = 128$). If the daughter nucleus is more tightly bound, the α decay is able to carry away more energy. (b) Neutron-capture cross sections of various nuclei. Note the decreases by roughly two orders of magnitude near $N = 50, 82,$ and 126 . (c) Change in the nuclear charge radius when $\Delta N = 2$. Note the sudden jumps at $20, 28, 50, 82,$ and 126 and compare with Figure 5.1. To emphasize the shell effects, the radius difference ΔR has been divided by the standard ΔR expected from the $A^{1/3}$ dependence. From E. B. Shera et al., *Phys. Rev. C* **14**, 731 (1976).

a collision. Thus the collisions cannot occur, and the nucleons can indeed orbit as if they were transparent to one another!

Shell Model Potential

The first step in developing the shell model is the choice of the potential, and we begin by considering two potentials for which we solved the three-dimensional Schrödinger equation in Chapter 2: the infinite well and the harmonic oscillator. The energy levels we obtained are shown in Figure 5.4. As in the case of atomic physics, the degeneracy of each level is the number of nucleons that can be put in each level, namely $2(2\ell + 1)$. The factor of $(2\ell + 1)$ arises from the m_ℓ degeneracy, and the additional factor of 2 comes from the m_s degeneracy. As in atomic physics, we use spectroscopic notation to label the levels, with one important exception: the index n is *not* the principal quantum number, but simply counts the number of levels with that ℓ value. Thus 1d means the first (lowest) d state, 2d means the second, and so on. (In atomic spectroscopic notation, there are no 1d or 2d states.) Figure 5.4 also shows the occupation

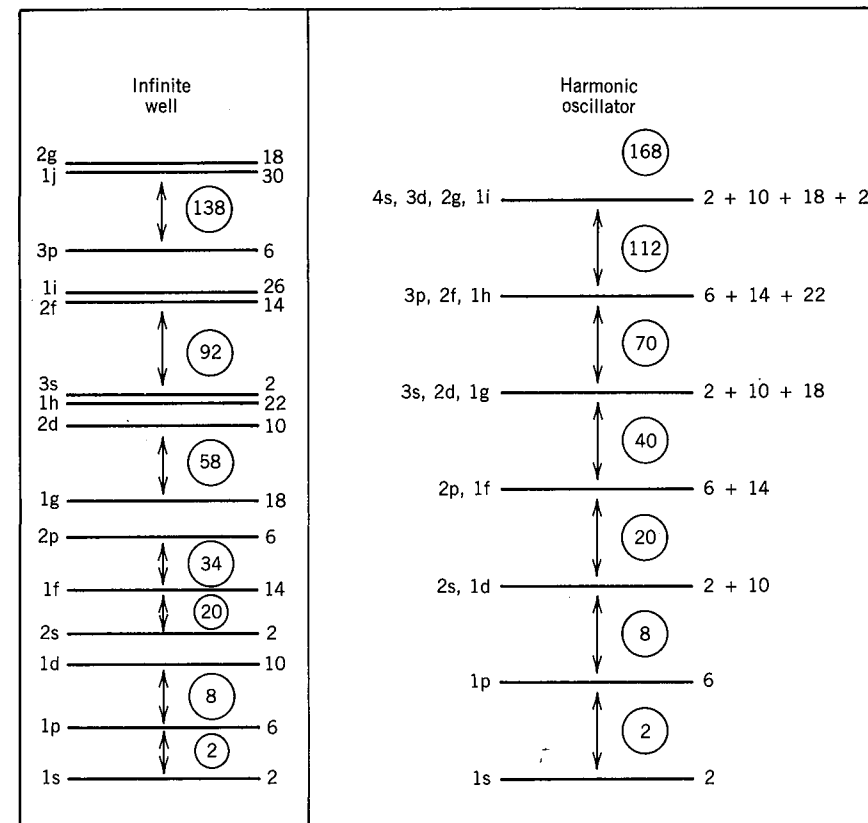


Figure 5.4 Shell structure obtained with infinite well and harmonic oscillator potentials. The capacity of each level is indicated to its right. Large gaps occur between the levels, which we associate with closed shells. The circled numbers indicate the total number of nucleons at each shell closure.

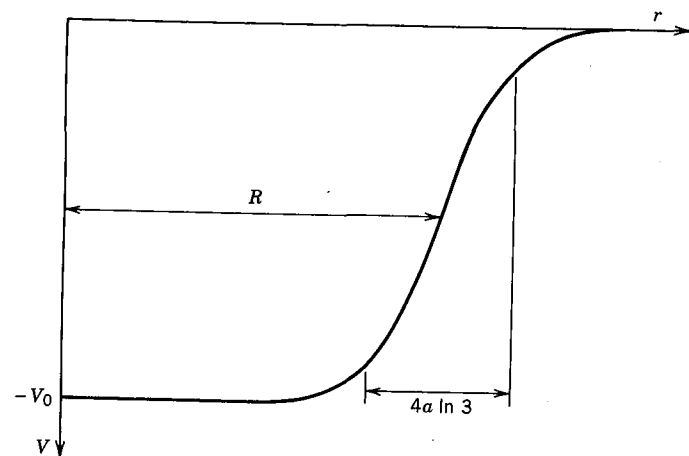


Figure 5.5 A realistic form for the shell-model potential. The "skin thickness" $4a \ln 3$ is the distance over which the potential changes from $0.9V_0$ to $0.1V_0$.

number of each level and the cumulative number of nucleons that would correspond to the filling of major shells. (Neutrons and protons, being nonidentical particles, are counted separately. Thus the 1s level can hold 2 protons as well as 2 neutrons.) It is encouraging to see the magic numbers of 2, 8, and 20 emerging in both of these schemes, but the higher levels do not correspond at all to the observed magic numbers.

As a first step in improving the model, we try to choose a more realistic potential. The infinite well is not a good approximation to the nuclear potential for several reasons: To separate a neutron or proton, we must supply enough energy to take it out of the well—an infinite amount! In addition, the nuclear potential does not have a sharp edge, but rather closely approximates the nuclear charge and matter distribution, falling smoothly to zero beyond the mean radius R . The harmonic oscillator, on the other hand, does not have a sharp enough edge, and it also requires infinite separation energies. Instead, we choose an intermediate form:

$$V(r) = \frac{-V_0}{1 + \exp[(r - R)/a]} \quad (5.1)$$

which is sketched in Figure 5.5. The parameters R and a give, respectively, the mean radius and skin thickness, and their values are chosen in accordance with the measurements discussed in Chapter 3: $R = 1.25A^{1/3}$ fm and $a = 0.524$ fm. The well depth V_0 is adjusted to give the proper separation energies and is of order 50 MeV. The resulting energy levels are shown in Figure 5.6; the effect of the potential, as compared with the harmonic oscillator (Figure 5.4) is to remove the ℓ degeneracies of the major shells. As we go higher in energy, the splitting becomes more and more severe, eventually becoming as large as the spacing between the oscillator levels themselves. Filling the shells in order with $2(2\ell + 1)$ nucleons, we again get the magic numbers 2, 8, and 20, but the higher magic numbers do not emerge from the calculations.

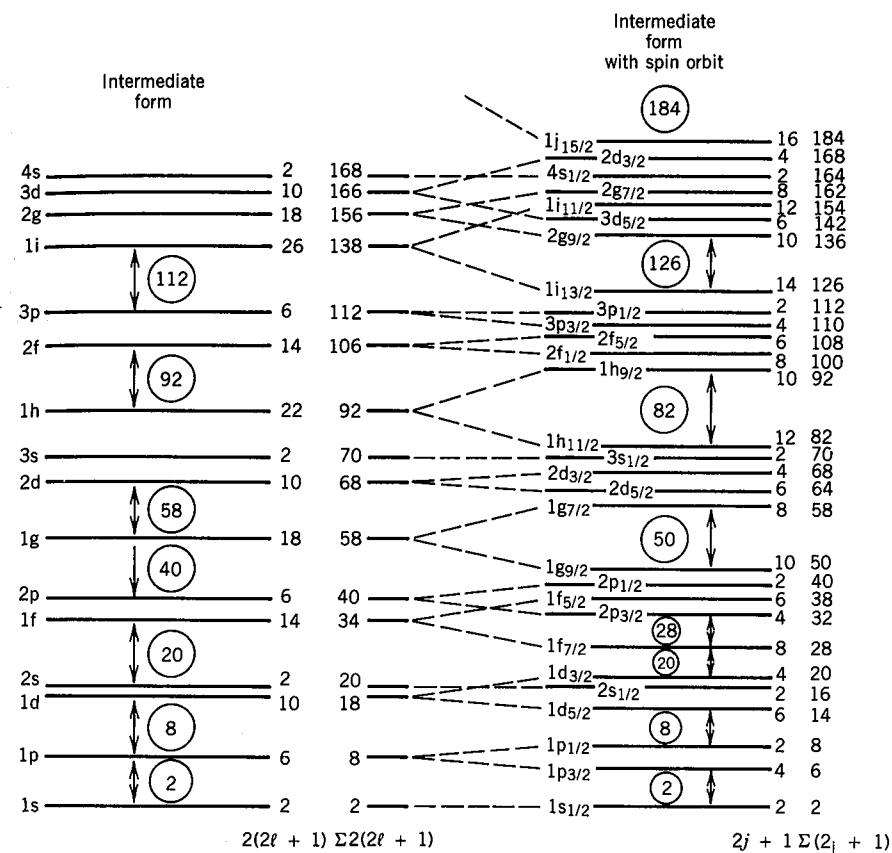


Figure 5.6 At the left are the energy levels calculated with the potential of Figure 5.5. To the right of each level are shown its capacity and the cumulative number of nucleons up to that level. The right side of the figure shows the effect of the spin-orbit interaction, which splits the levels with $\ell > 0$ into two new levels. The shell effect is quite apparent, and the magic numbers are exactly reproduced.

Spin-Orbit Potential

How can we modify the potential to give the proper magic numbers? We certainly cannot make a radical change in the potential, because we do not want to destroy the physical content of the model—Equation 5.1 is already a very good guess at how the nuclear potential *should* look. It is therefore necessary to add various terms to Equation 5.1 to try to improve the situation. In the 1940s, many unsuccessful attempts were made at finding the needed correction; success was finally achieved by Mayer, Haxel, Suess, and Jensen who showed in 1949 that the inclusion of a *spin-orbit* potential could give the proper separation of the subshells.

Once again, we are borrowing an idea from our colleagues, the atomic physicists. In atomic physics the spin-orbit interaction, which causes the observed fine structure of spectral lines, comes about because of the electromagnetic interaction of the electron's magnetic moment with the magnetic field generated by its motion about the nucleus. The effects are typically very small, perhaps one

part in 10^5 in the spacing of atomic levels. No such electromagnetic interaction would be strong enough to give the substantial changes in the *nuclear* level spacing needed to generate the observed magic numbers. Nevertheless we adopt the concept of a *nuclear* spin-orbit force of the same form as the atomic spin-orbit force but certainly *not* electromagnetic in origin. In fact, we know from the scattering experiments discussed in Chapter 4 that there is strong evidence for a nucleon-nucleon spin-orbit force.

The spin-orbit interaction is written as $V_{so}(r)\ell \cdot s$, but the form of $V_{so}(r)$ is not particularly important. It is the $\ell \cdot s$ factor that causes the reordering of the levels. As in atomic physics, in the presence of a spin-orbit interaction it is appropriate to label the states with the *total angular momentum* $j = \ell + s$. A single nucleon has $s = \frac{1}{2}$, so the possible values of the total angular momentum quantum number are $j = \ell + \frac{1}{2}$ or $j = \ell - \frac{1}{2}$ (except for $\ell = 0$, in which case only $j = \frac{1}{2}$ is allowed). The expectation value of $\ell \cdot s$ can be calculated using a common trick. We first evaluate $j^2 = (\ell + s)^2$:

$$j^2 = \ell^2 + 2\ell \cdot s + s^2 \quad (5.2)$$

$$\ell \cdot s = \frac{1}{2}(j^2 - \ell^2 - s^2)$$

Putting in the expectation values gives

$$\langle \ell \cdot s \rangle = \frac{1}{2}[j(j+1) - \ell(\ell+1) - s(s+1)]\hbar^2 \quad (5.3)$$

Consider a level such as the $1f$ level ($\ell = 3$), which has a degeneracy of $2(2\ell + 1) = 14$. The possible j values are $\ell \pm \frac{1}{2} = \frac{5}{2}$ or $\frac{7}{2}$. Thus we have the levels $1f_{5/2}$ and $1f_{7/2}$. The degeneracy of each level is $(2j + 1)$, which comes from the m_j values. (With spin-orbit interactions, m_s and m_ℓ are no longer "good" quantum numbers and can no longer be used to label states or to count degeneracies.) The capacity of the $1f_{5/2}$ level is therefore 6 and that of $1f_{7/2}$ is 8, giving again 14 states (the number of possible states must be preserved; we are only grouping them differently). For the $1f_{5/2}$ and $1f_{7/2}$ states, which are known as a spin-orbit pair or doublet, there is an energy separation that is proportional to the value of $\langle \ell \cdot s \rangle$ for each state. Indeed, for any pair of states with $\ell > 0$, we can compute the energy difference using Equation 5.3:

$$\langle \ell \cdot s \rangle_{j=\ell+1/2} - \langle \ell \cdot s \rangle_{j=\ell-1/2} = \frac{1}{2}(2\ell + 1)\hbar^2 \quad (5.4)$$

The energy splitting increases with increasing ℓ . Consider the effect of choosing $V_{so}(r)$ to be negative, so that the member of the pair with the larger j is pushed downward. Figure 5.6 shows the effect of this splitting. The $1f_{7/2}$ level now appears in the gap between the second and third shells; its capacity of 8 nucleons gives the magic number 28. (The p and d splittings do not result in any major regrouping of the levels.) The next major effect of the spin-orbit term is on the $1g$ level. The $1g_{9/2}$ state is pushed down all the way to the next lower major shell; its capacity of 10 nucleons adds to the previous total of 40 for that shell to give the magic number of 50. A similar effect occurs at the top of each major shell. In each case the lower energy member of the spin-orbit pair from the next shell is pushed down into the lower shell, and the remaining magic numbers follow exactly as expected. (We even predict a new one, at 184, which has not yet been seen.)

As an example of the application of the shell model, consider the filling of levels needed to produce $^{15}_8\text{O}$ and $^{17}_8\text{O}$. The 8 protons fill a major shell and do not

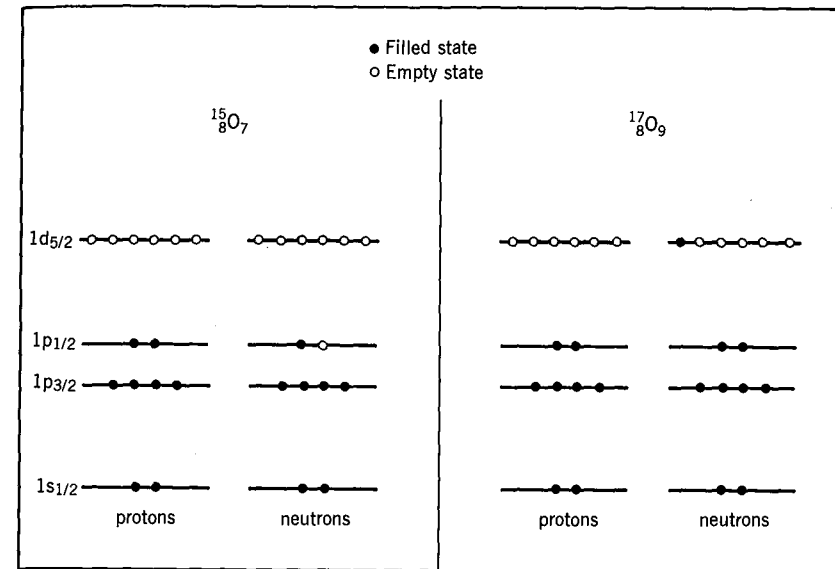


Figure 5.7 The filling of shells in ^{15}O and ^{17}O . The filled proton shells do not contribute to the structure; the properties of the ground state are determined primarily by the odd neutron.

contribute to the structure. Figure 5.7 shows the filling of levels. The extreme limit of the shell model asserts that only the single unpaired nucleon determines the properties of the nucleus. In the case of ^{15}O , the unpaired neutron is in the $p_{1/2}$ shell; we would therefore predict that the ground state of ^{15}O has spin $\frac{1}{2}$ and odd parity, since the parity is determined by $(-1)^\ell$. The ground state of ^{17}O should be characteristic of a $d_{5/2}$ neutron with spin $\frac{5}{2}$ and even parity. These two predictions are in exact agreement with the observed spin-parity assignments, and in fact similar agreements are found throughout the range of odd- A nuclei where the shell model is valid (generally $A < 150$ and $190 < A < 220$, for reasons to be discussed later in this chapter). This success in accounting for the observed ground-state spin-parity assignments was a great triumph for the shell model.

Magnetic Dipole Moments

Another case in which the shell model gives a reasonable (but not so exact) agreement with observed nuclear properties is in the case of magnetic dipole moments. You will recall from Chapter 3 that the magnetic moment is computed from the expectation value of the magnetic moment operator in the state with maximum z projection of angular momentum. Thus, including both ℓ and s terms, we must evaluate

$$\mu = \mu_N(g_\ell \ell_z + g_s s_z)/\hbar \quad (5.5)$$

when $j_z = j\hbar$. This cannot be evaluated directly, since ℓ_z and s_z do not have precisely defined values when we work in a system in which j is precisely defined. We can rewrite this expression, using $j = \ell + s$, as

$$\mu = [g_\ell j_z + (g_s - g_\ell)s_z]\mu_N/\hbar \quad (5.6)$$

and, taking the expectation value when $j_z = j\hbar$, the result is

$$\langle \mu \rangle = [g_\ell j + (g_s - g_\ell)\langle s_z \rangle/\hbar]\mu_N \quad (5.7)$$

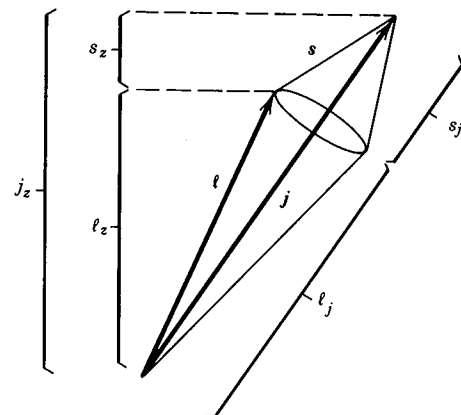


Figure 5.8 As the total angular momentum j precesses about the z axis keeping j_z constant, the vectors ℓ and s precess about j . The components of ℓ and s along j remain constant, but ℓ_z and s_z vary.

The expectation value of $\langle s_z \rangle$ can be quickly computed by recalling that j is the only vector of interest in this problem—the ℓ and s vectors are meaningful only in their relationship to j . Specifically, when we compute $\langle s_z \rangle$ the only surviving part will be from the component of s along j , as suggested by the vector diagram of Figure 5.8. The instantaneous value of s_z varies, but its component along j remains constant. We therefore need an expression for the vector s_j , the component of s along j . The unit vector along j is $j/|j|$, and the component of s along j is $|s \cdot j|/|j|$. The vector s_j is therefore $j|s \cdot j|/|j|^2$, and replacing all quantities by their expectation values gives

$$\langle s_z \rangle = \frac{j}{2j(j+1)} [j(j+1) - \ell(\ell+1) + s(s+1)] \hbar \quad (5.8)$$

where $s \cdot j = s \cdot (\ell + s)$ is computed using Equation 5.3. Thus for $j = \ell + \frac{1}{2}$, $\langle s_z \rangle = \hbar/2$, while for $j = \ell - \frac{1}{2}$ we have $\langle s_z \rangle = -\hbar j/2(j+1)$. The corresponding magnetic moments are

$$\begin{aligned} j = \ell + \frac{1}{2} \quad \langle \mu \rangle &= [g_\ell(j - \frac{1}{2}) + \frac{1}{2}g_s] \mu_N \\ j = \ell - \frac{1}{2} \quad \langle \mu \rangle &= \left[g_\ell \frac{j(j + \frac{3}{2})}{(j+1)} - \frac{1}{2} \frac{1}{j+1} g_s \right] \mu_N \end{aligned} \quad (5.9)$$

Figure 5.9 shows a comparison of these calculated values with measured values for shell-model odd- A nuclei. The computed values are shown as solid lines and are known as the Schmidt lines; this calculation was first done by Schmidt in 1937. The experimental values fall within the limits of the Schmidt lines, but are generally smaller in magnitude and have considerable scatter. One defect of this theory is the assumption that g_s for a nucleon in a nucleus is the same as g_s for a free nucleon. We discussed in Chapter 3 how the spin g factors of nucleons differ considerably from the value of 2 expected for “elementary” spin- $\frac{1}{2}$ particles. If we regard the substantial differences as arising from the “meson cloud” that surrounds the nucleon, then it is not at all surprising that the meson cloud in nuclei, where there are other surrounding nucleons and mesons, differs from what it is for free nucleons. It is customary to account for this effect by (somewhat

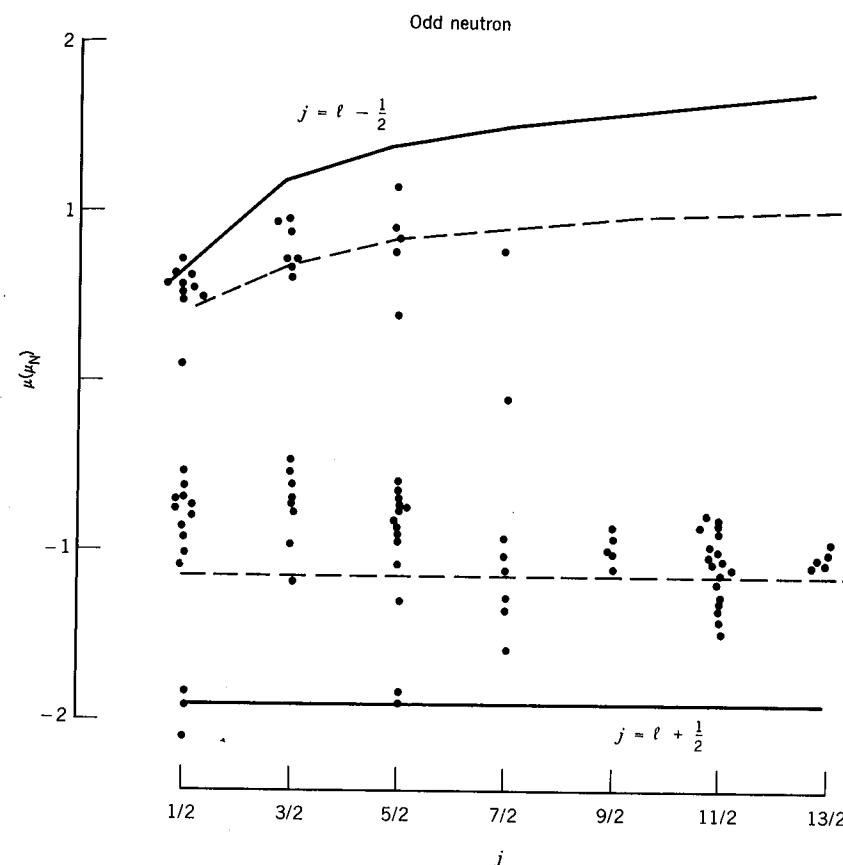


Figure 5.9 Experimental values for the magnetic moments of odd-neutron and odd-proton shell-model nuclei. The Schmidt lines are shown as solid for $g_s = g_s(\text{free})$ and dashed for $g_s = 0.6g_s(\text{free})$.

arbitrarily) reducing the g_s factor; for example, the lines for $g_s = 0.6g_s(\text{free})$ are shown in Figure 5.9. The overall agreement with experiment is better, but the scatter of the points suggests that the model is oversimplifying the calculation of magnetic moments. Nevertheless, the success in indicating the general trend of the observed magnetic moments suggests that the shell model gives us at least an approximate understanding of the structure of these nuclei.

Electric Quadrupole Moments

The calculation of electric quadrupole moments in the shell model is done by evaluating the electric quadrupole operator, $3z^2 - r^2$, in a state in which the total angular momentum of the odd particle has its maximum projection along the z axis (that is, $m_j = +j$). Let's assume for now that the odd particle is a proton. If its angular momentum is aligned (as closely as quantum mechanics allows) with the z axis, then it must be orbiting mostly in the xy plane. As we indicated in the discussion following Equation 3.36, this would give a negative quadrupole

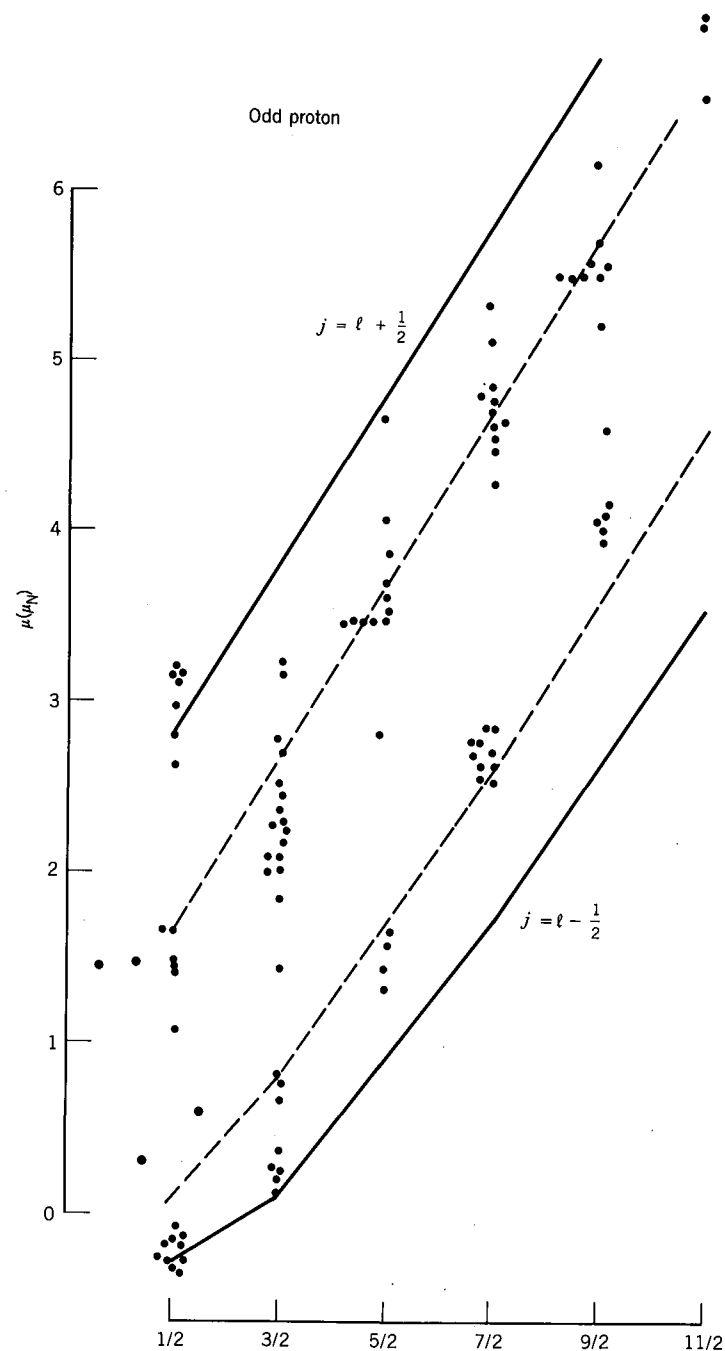


Figure 5.9 Continued.

Table 5.1 Shell-Model Quadrupole Moments

Shell-Model State	Calculated Q (single proton)	Measured Q			
		Single Particle		Single Hole	
		p	n	p	n
$1p_{3/2}$	-0.013	-0.0366(${}^7\text{Li}$)		+0.0407(${}^{11}\text{B}$)	+0.053(${}^9\text{Be}$)
$1d_{5/2}$	-0.036	-0.12(${}^{19}\text{F}$)	-0.026(${}^{17}\text{O}$)	+0.140(${}^{27}\text{Al}$)	+0.201(${}^{25}\text{Mg}$)
$1d_{3/2}$	-0.037	-0.08249(${}^{35}\text{Cl}$)	-0.064(${}^{33}\text{S}$)	+0.056(${}^{39}\text{K}$)	+0.45(${}^{35}\text{S}$)
$1f_{7/2}$	-0.071	-0.26(${}^{43}\text{Sc}$)	-0.080(${}^{41}\text{Ca}$)	+0.40(${}^{59}\text{Co}$)	+0.24(${}^{49}\text{Ti}$)
$2p_{3/2}$	-0.055	-0.209(${}^{63}\text{Cu}$)	-0.0285(${}^{53}\text{Cr}$)	+0.195(${}^{67}\text{Ga}$)	+0.20(${}^{57}\text{Fe}$)
$1f_{5/2}$	-0.086		-0.20(${}^{61}\text{Ni}$)	+0.274(${}^{85}\text{Rb}$)	+0.15(${}^{67}\text{Zn}$)
$1g_{9/2}$	-0.13	-0.32(${}^{93}\text{Nb}$)	-0.17(${}^{73}\text{Ge}$)	+0.86(${}^{115}\text{In}$)	+0.45(${}^{85}\text{Kr}$)
$1g_{7/2}$	-0.14	-0.49(${}^{123}\text{Sb}$)		+0.20(${}^{139}\text{La}$)	
$2d_{5/2}$	-0.12	-0.36(${}^{121}\text{Sb}$)	-0.236(${}^{91}\text{Zr}$)		+0.44(${}^{111}\text{Cd}$)

Data for this table are derived primarily from the compilation of V. S. Shirley in the *Table of Isotopes*, 7th ed. (New York: Wiley, 1978). The uncertainties in the values are typically a few parts in the last quoted significant digit.

moment of the order of $Q \approx -\langle r^2 \rangle$. Some experimental values of quadrupole moments of nuclei that have one proton beyond a filled subshell are listed in Table 5.1. Values of $\langle r^2 \rangle$ range from 0.03 b for $A = 7$ to 0.3 b for $A = 209$, and thus the measured values are in good agreement with our expectations.

A more refined quantum mechanical calculation gives the single-particle quadrupole moment of an odd proton in a shell-model state j :

$$\langle Q_{sp} \rangle = -\frac{2j-1}{2(j+1)} \langle r^2 \rangle \quad (5.10)$$

For a uniformly charged sphere, $\langle r^2 \rangle = \frac{3}{5}R^2 = \frac{3}{5}R_0^2 A^{2/3}$. Using these results, we can compute the quadrupole moments for the nuclei shown in Table 5.1. The calculated values have the correct sign but are about a factor of 2-3 too small.

A more disturbing difficulty concerns nuclei with an odd neutron. An uncharged neutron outside a filled subshell should have no quadrupole moment at all. From Table 5.1 we see that the odd-neutron values are generally smaller than the odd-proton values, but they are most definitely not zero.

When a subshell contains more than a single particle, all of the particles in the subshell can contribute to the quadrupole moment. Since the capacity of any subshell is $2j+1$, the number of nucleons in an unfilled subshell will range from 1 to $2j$. The corresponding quadrupole moment is

$$\langle Q \rangle = \langle Q_{sp} \rangle \left[1 - 2 \frac{n-1}{2j-1} \right] \quad (5.11)$$

where n is the number of nucleons in the subshell ($1 \leq n \leq 2j$) and Q_{sp} is the

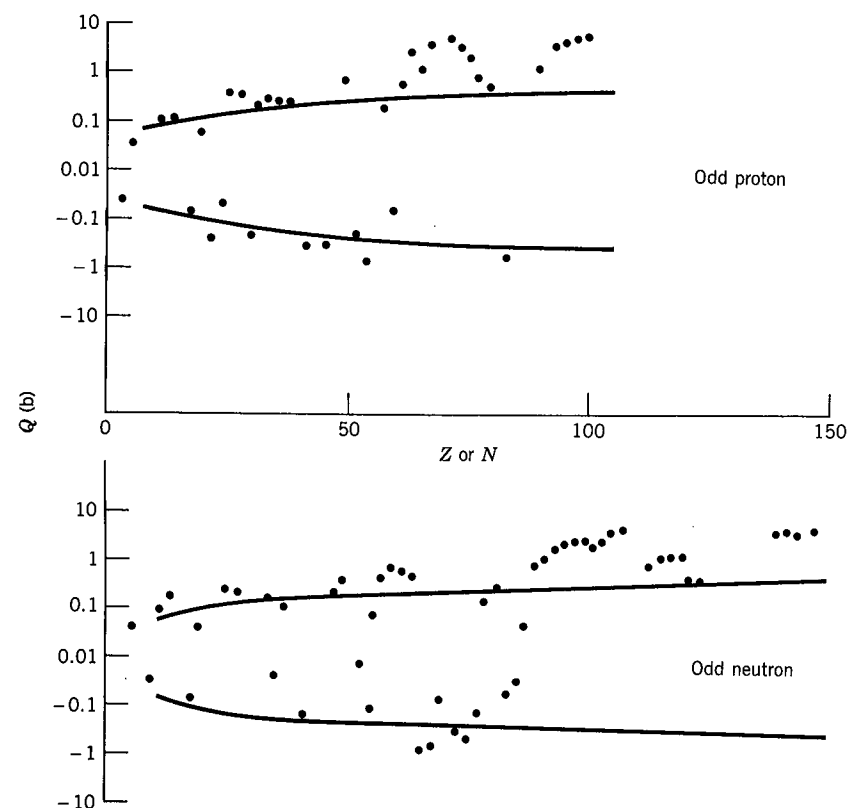


Figure 5.10 Experimental values of electric quadrupole moments of odd-neutron and odd-proton nuclei. The solid lines show the limits $Q \sim \langle r^2 \rangle$ expected for shell-model nuclei. The data are within the limits, except for the regions $60 < Z < 80$, $Z > 90$, $90 < N < 120$, and $N > 140$, where the experimental values are more than an order of magnitude larger than predicted by the shell model.

single-particle quadrupole moment given in Equation 5.10. When $n = 1$, $Q = Q_{sp}$, but when $n = 2j$ (corresponding to a subshell that lacks only one nucleon from being filled), $Q = -Q_{sp}$. Table 5.1 shows the quadrupole moments of these so-called “hole” states, and you can see that to a very good approximation, $Q(\text{particle}) = -Q(\text{hole})$. In particular, the quadrupole moments of the hole states are positive and opposite in sign to the quadrupole moments of the particle states.

Before we are overcome with enthusiasm with the success of this simple model, let us look at the entire systematic behavior of the quadrupole moments. Figure 5.10 summarizes the measured quadrupole moments of the ground states of odd-mass nuclei. There is some evidence for the change in sign of Q predicted by Equation 5.11, but the situation is not entirely symmetric—there are far more positive than negative quadrupole moments. Even worse, the model fails to predict the extremely large quadrupole moments of several barns observed for certain heavy nuclei. The explanations for these failures give us insight into other aspects of nuclear structure that cannot be explained within the shell model. We discuss these new features in the last two sections of this chapter.

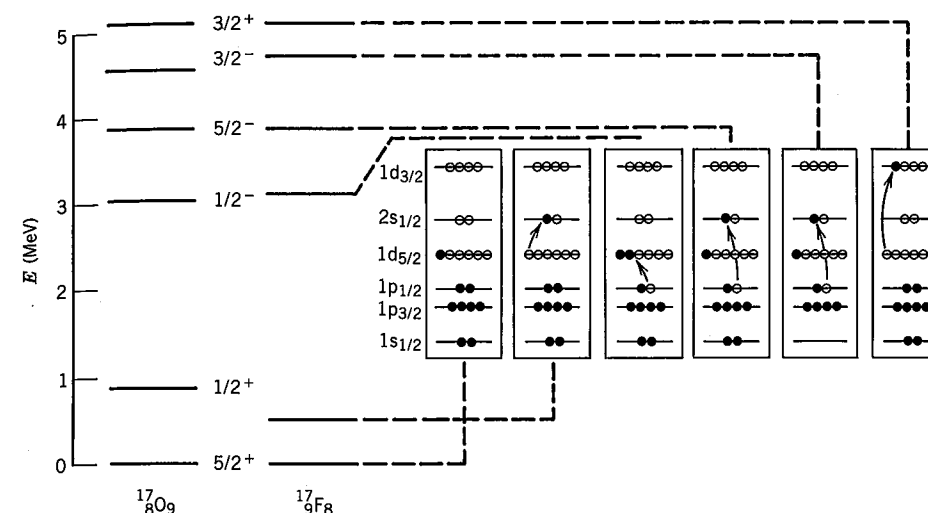


Figure 5.11 Shell-model interpretation of the levels of ^{17}O and ^{17}F . All levels below about 5 MeV are shown, and the similarity between the levels of the two nuclei suggests they have common structures, determined by the valence nucleons. The even-parity states are easily explained by the excitation of the single odd nucleon from the $d_{5/2}$ ground state to $2s_{1/2}$ or $1d_{3/2}$. The odd-parity states have more complicated structures; one possible configuration is shown, but others are also important.

Valence Nucleons

The shell model, despite its simplicity, is successful in accounting for the spins and parities of nearly all odd- A ground states, and is somewhat less successful (but still satisfactory) in accounting for magnetic dipole and electric quadrupole moments. The particular application of the shell model that we have considered is known as the *extreme independent particle model*. The basic assumption of the extreme independent particle model is that all nucleons but one are paired, and the nuclear properties arise from the motion of the single unpaired nucleon. This is obviously an oversimplification, and as a next better approximation we can treat all of the particles in the unfilled subshell. Thus in a nucleus such as $^{43}_{20}\text{Ca}_{23}$, with three neutrons beyond the closed shell at $N = 20$, the extreme version of the shell model considers only the 23rd neutron, but a more complete shell model calculation should consider all three valence neutrons. For $^{45}_{22}\text{Ti}_{23}$, we should take into account all five particles (2 protons, 3 neutrons) beyond the closed shells at $Z = 20$ and $N = 20$.

If the extreme independent particle model were valid, we should be able to reproduce diagrams like Figure 5.6 by studying the excited states of nuclei. Let's examine some examples of this procedure. Figure 5.11 shows some of the excited states of $^{17}\text{O}_9$ and $^{17}\text{F}_8$, each of which has only one nucleon beyond a doubly magic ($Z = 8$, $N = 8$) core. The ground state is $\frac{5}{2}^+$, as expected for the $d_{5/2}$ shell-model state of the 9th nucleon. From Figure 5.6 we would expect to find excited states with spin-parity assignments of $\frac{1}{2}^+$ and $\frac{3}{2}^+$, corresponding to the $1s_{1/2}$ and $1d_{3/2}$ shell-model levels. According to this assumption, when we add

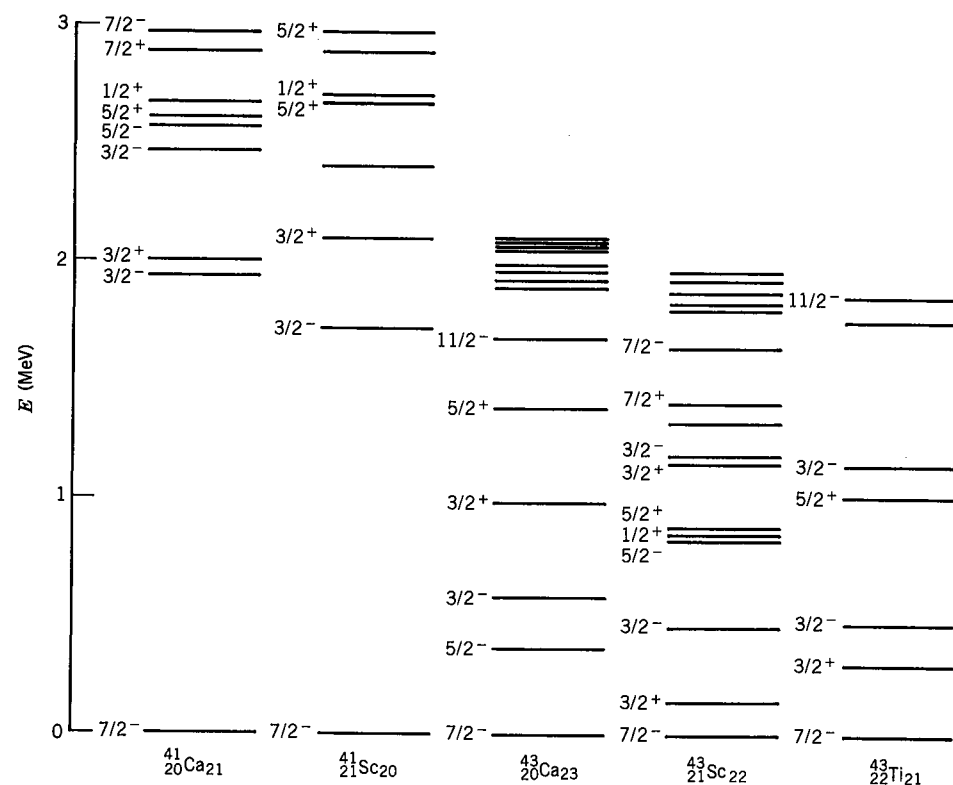


Figure 5.12 Energy levels of nuclei with odd particles in the $1f_{7/2}$ shell.

energy to the nucleus, the core remains inert and the odd particle absorbs the energy and moves to higher shell-model levels. The expected $\frac{1}{2}^+$ shell-model state appears as the first excited state, and the $\frac{3}{2}^+$ state is much higher, but how can we account for $\frac{1}{2}^-$, $\frac{3}{2}^-$, and $\frac{5}{2}^-$? (The negative parity $2p_{1/2}$, $2p_{3/2}$, and $1f_{5/2}$ shell-model states are well above the $1d_{3/2}$ state, which should therefore appear lower.) Figure 5.11 shows one possible explanation for the $\frac{1}{2}^-$ state: instead of exciting the odd nucleon to a higher state, we break the pair in the $1p_{1/2}$ level and excite one of the nucleons to pair with the nucleon in the $d_{5/2}$ level. The odd nucleon is now in the $1p_{1/2}$ state, giving us a $\frac{1}{2}^-$ excited state. (Because the pairing energy increases with ℓ , it is actually energetically favorable to break an $\ell = 1$ pair and form an $\ell = 2$ pair.) Verification of this hypothesis requires that we determine by experiment whether the properties of the $\frac{1}{2}^-$ state agree with those expected for a $p_{1/2}$ shell-model state. A similar assumption might do as well for the $\frac{3}{2}^-$ state (breaking a $p_{3/2}$ pair), but that still does not explain the $\frac{5}{2}^-$ state or the many other excited states.

In Figure 5.12, we show a similar situation for nuclei in the $1f_{7/2}$ shell. The $\frac{7}{2}^-$ ground state ($1f_{7/2}$) and the $\frac{3}{2}^-$ excited state ($2p_{3/2}$) appear as expected in the nuclei ^{41}Ca and ^{41}Sc , each of which has only a single nucleon beyond a doubly magic ($Z = 20$, $N = 20$) core. In ^{43}Ca , the structure is clearly quite different from that of ^{41}Ca . Many more low-lying states are present. These states come

from the coupling of three particles in the $1f_{7/2}$ shell and illustrate the difference between the complete shell model and its extreme independent particle limit. If only the odd particle were important, ^{43}Ca should be similar to ^{41}Ca . In ^{43}Sc , you can see how the 21st and 22nd neutrons, which would be ignored in the extreme independent particle limit, have a great effect on the structure. Similarly, the level scheme of ^{43}Ti shows that the 21st and 22nd protons have a great effect on the shell-model levels of the 21st neutron.

In addition to spin-parity assignments, magnetic dipole moments, electric quadrupole moments, and excited states, the shell model can also be used to calculate the probability of making a transition from one state to another as a result of a radioactive decay or a nuclear reaction. We examine the shell model predictions for these processes in later chapters.

Let's conclude this discussion of the shell model with a brief discussion of the question we raised at the beginning—how can we be sure that the very concept of a nucleon with definite orbital properties remains valid deep in the nuclear interior? After all, many of the tests of the shell model involve such nuclear properties as the spin and electromagnetic moments of the valence particles, all of which are concentrated near the nuclear surface. Likewise, many experimental probes of the nucleus, including other particles that feel the nuclear force, tell us mostly about the surface properties. To answer the question we have proposed,

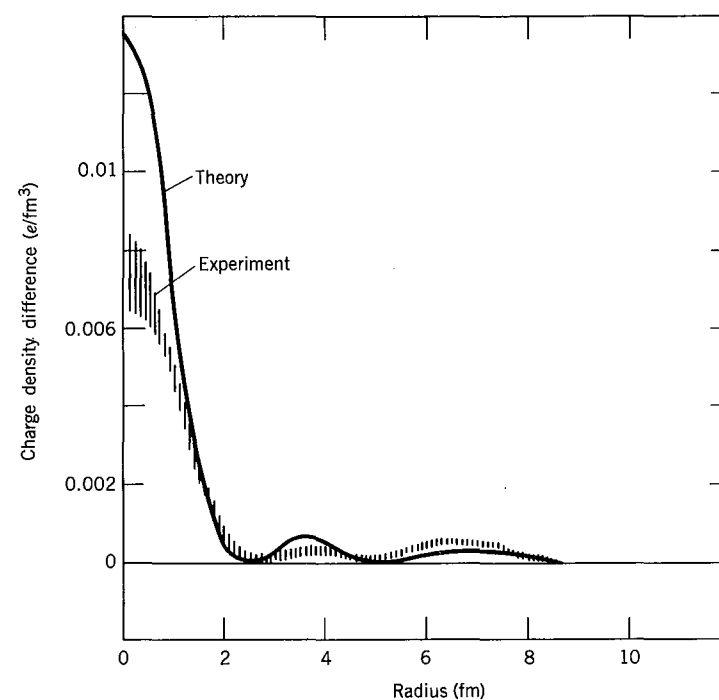


Figure 5.13 The difference in charge density between ^{205}Tl and ^{206}Pb , as determined by electron scattering. The curve marked "theory" is just the square of a harmonic oscillator $3s$ wave function. The theory reproduces the variations in the charge density extremely well. Experimental data are from J. M. Cavedon et al., *Phys. Rev. Lett.* **49**, 978 (1982).

what is needed is a probe that reaches deep into the nucleus, and we must use that probe to measure a nuclear property that characterizes the interior of the nucleus and not its surface. For a probe we choose high-energy electrons, as we did in studying the nuclear charge distribution in Chapter 3. The property that is to be measured is the charge density of a single nucleon in its orbit, which is equivalent to the square of its wave function, $|\psi|^2$. Reviewing Figure 2.12 we recall that only s-state wave functions penetrate deep into the nuclear interior; for other states $\psi \rightarrow 0$ as $r \rightarrow 0$. For our experiment we therefore choose a nucleus such as $^{205}_{81}\text{Tl}_{124}$, which lacks a single proton in the $3s_{1/2}$ orbit from filling all subshells below the $Z = 82$ gap. How can we measure the contribution of just the $3s_{1/2}$ proton to the charge distribution and ignore the other protons? We can do so by measuring the *difference* in charge distribution between ^{205}Tl and $^{206}\text{Pb}_{124}$, which has the filled proton shell. Any difference between the charge distributions of these two nuclei must be due to the extra $3s_{1/2}$ proton in ^{206}Pb . Figure 5.13 shows the experimentally observed difference in the charge distributions as measured in a recent experiment. The comparison with $|\psi|^2$ for a 3s wave function is very successful (using the same harmonic oscillator wave function plotted in Figure 2.12, except that here we plot $|\psi|^2$, not r^2R^2), thus confirming the validity of the assumption about nucleon orbits retaining their character deep in the nuclear interior. From such experiments we gain confidence that the independent-particle description, so vital to the shell model, is not just a convenience for analyzing measurements near the nuclear surface, but instead is a valid representation of the behavior of nucleons throughout the nucleus.

5.2 EVEN-Z, EVEN-N NUCLEI AND COLLECTIVE STRUCTURE

Now let's try to understand the structure of nuclei with even numbers of protons and neutrons (known as *even-even* nuclei). As an example, consider the case of ^{130}Sn , shown in Figure 5.14. The shell model predicts that all even-even nuclei will have 0^+ (spin 0, even parity) ground states, because all of the nucleons are paired. According to the shell model, the 50 protons of ^{130}Sn fill the $g_{9/2}$ shell and the 80 neutrons lack 2 from filling the $h_{11/2}$ shell to complete the magic number of $N = 82$. To form an excited state, we can break one of the pairs and excite a nucleon to a higher level; the coupling between the two odd nucleons then determines the spin and parity of the levels. Promoting one of the $g_{9/2}$ protons or $h_{11/2}$ neutrons to a higher level requires a great deal of energy, because the gap between the major shells must be crossed (see Figure 5.6). We therefore expect that the major components of the wave functions of the lower excited states will consist of neutron excitation within the last occupied major shell. For example, if we assume that the ground-state configuration of ^{130}Sn consists of filled $s_{1/2}$ and $d_{3/2}$ subshells and 10 neutrons (out of a possible 12) occupying the $h_{11/2}$ subshell, then we could form an excited state by breaking the $s_{1/2}$ pair and promoting one of the $s_{1/2}$ neutrons to the $h_{11/2}$ subshell. Thus we would have one neutron in the $s_{1/2}$ subshell and 11 neutrons in the $h_{11/2}$ subshell. The properties of such a system would be determined mainly by the coupling of the $s_{1/2}$ neutron with the unpaired $h_{11/2}$ neutron. Coupling angular momenta j_1 and j_2 in quantum mechanics gives values from the sum $j_1 + j_2$ to the difference $|j_1 - j_2|$ in integer steps. In this case the possible resultants are $\frac{11}{2} + \frac{1}{2} = 6$ and $\frac{11}{2} - \frac{1}{2} = 5$. Another possibility would be to break one of the $d_{3/2}$ pairs and again place an odd neutron in the $h_{11/2}$ subshell. This would give resulting angular momenta ranging from $\frac{11}{2} + \frac{3}{2} = 7$ to $\frac{11}{2} - \frac{3}{2} = 4$. Because the $s_{1/2}$ and $d_{3/2}$ neutrons have even parity and the $h_{11/2}$ neutron has odd parity, all of these couplings will give states with odd parity. If we examine the ^{130}Sn level scheme, we do indeed see several odd parity states with spins in the range of 4–7 with energies about 2 MeV. This energy is characteristic of what is needed to break a pair and excite a particle within a shell, and so we have a strong indication that we understand those states. Another possibility to form excited states would be to break one of the $h_{11/2}$ pairs and, keeping both members of the pair in the $h_{11/2}$ subshell, merely recouple them to a spin different from 0; according to the angular momentum coupling rules, the possibilities would be anything from $\frac{11}{2} + \frac{11}{2} = 11$ to $\frac{11}{2} - \frac{11}{2} = 0$. The two $h_{11/2}$ neutrons must be treated as identical particles and must therefore be described by a properly symmetrized wave function. This requirement restricts the resultant coupled spin to even values, and thus the possibilities are $0^+, 2^+, 4^+, 6^+, 8^+, 10^+$. There are several candidates for these states in the 2-MeV region, and here again the shell model seems to give us a reasonable description of the level structure.

A major exception to this successful interpretation is the 2^+ state at about 1.2 MeV. Restricting our discussion to the neutron states, what are the possible ways to couple two neutrons to get 2^+ ? As discussed above, the two $h_{11/2}$ neutrons can couple to 2^+ . We can also excite a pair of $d_{3/2}$ neutrons to the $h_{11/2}$ subshell

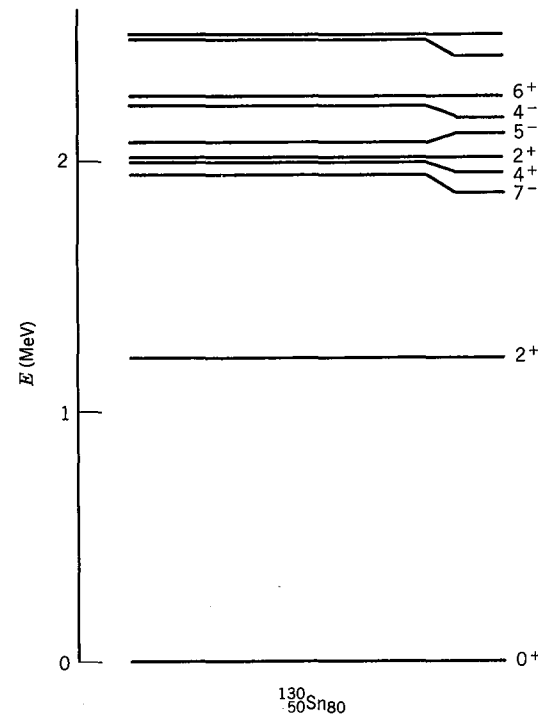


Figure 5.14 The low-lying energy levels of ^{130}Sn .

(thus filling that shell and making an especially stable configuration), then break the coupling of the two remaining $d_{3/2}$ neutrons and recouple them to 2^+ . Yet another possibility would be to place the pair of $s_{1/2}$ neutrons into the $h_{11/2}$ subshell, and excite one of the $d_{3/2}$ neutrons to the $s_{1/2}$ subshell. We would then have an odd neutron in each of the $d_{3/2}$ and $s_{1/2}$ subshells, which could couple to 2^+ . However, in all these cases we must first break a pair, and thus the resulting states would be expected at about 2 MeV.

Of course, the shell-model description is only an approximation, and it is unlikely that "pure" shell-model states will appear in a complex level scheme. A better approach is to recognize that if we wish to use the shell model as a means to interpret the structure, then the physical states must be described as combinations of shell-model states, thus:

$$\begin{aligned} \psi(2^+) = & a\psi(\nu h_{11/2} \oplus \nu h_{11/2}) + b\psi(\nu d_{3/2} \oplus \nu d_{3/2}) \\ & + c\psi(\nu d_{3/2} \oplus \nu s_{1/2}) + \dots \end{aligned} \quad (5.12)$$

where ν stands for neutron and the \oplus indicates that we are doing the proper angular momentum coupling to get the 2^+ resultant. The puzzle of the low-lying 2^+ state can now be rephrased as follows: Each of the constituent states has an energy of about 2 MeV. What is it about the nuclear interaction that gives the right mixture of expansion coefficients a, b, c, \dots to force the state down to an energy of 1.2 MeV?

Our first thought is that this structure may be a result of the particular shell-model levels occupied by the valence particles of ^{130}Sn . We therefore examine other even-even nuclei and find this remarkable fact: of the hundreds of known even-even nuclei in the shell-model region, *each one* has an "anomalous" 2^+ state at an energy at or below one-half of the energy needed to break a pair. In all but a very few cases, this 2^+ state is the lowest excited state. The occurrence of this state is thus not an accident resulting from the shell-model structure of ^{130}Sn . Instead it is a *general property* of even- Z , even- N nuclei, valid throughout the entire mass range, independent of which particular shell-model states happen to be occupied. We will see that there are other general properties that are common to all nuclei, and it is reasonable to identify those properties not with the motion of a few valence nucleons, but instead with the entire nucleus. Such properties are known as *collective properties* and their origin lies in the nuclear collective motion, in which many nucleons contribute cooperatively to the nuclear properties. The collective properties vary smoothly and gradually with mass number and are mostly independent of the number and kind of valence nucleons outside of filled subshells (although the valence nucleons may contribute shell structure that couples with the collective structure).

In Figures 5.15 and 5.16 are shown four different properties of even-even nuclei that reveal collective behavior. The energy of the first 2^+ excited state (Figure 5.15a) seems to decrease rather smoothly as a function of A (excepting the regions near closed shells). The region from about $A = 150$ to $A = 190$ shows values of $E(2^+)$ that are both exceptionally small and remarkably constant. Again excepting nuclei near closed shells, the ratio $E(4^+)/E(2^+)$ (Figure 5.15b)

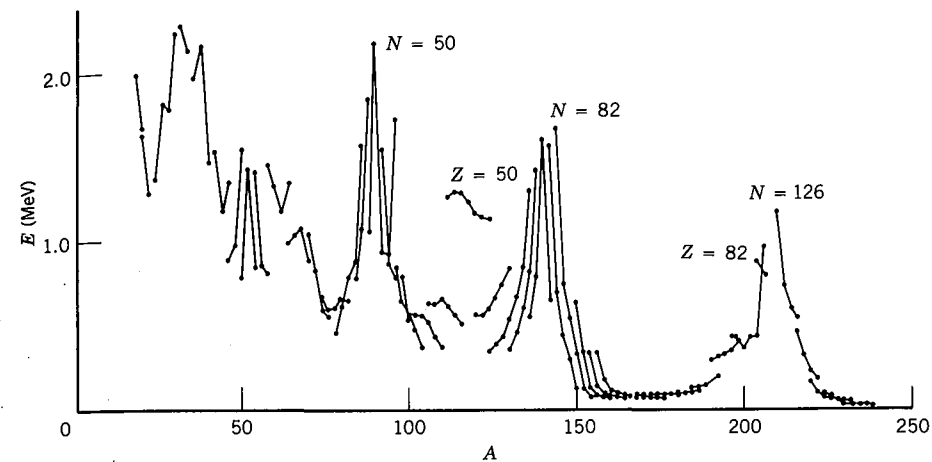


Figure 5.15a Energies of lowest 2^+ states of even- Z , even- N nuclei. The lines connect sequences of isotopes.

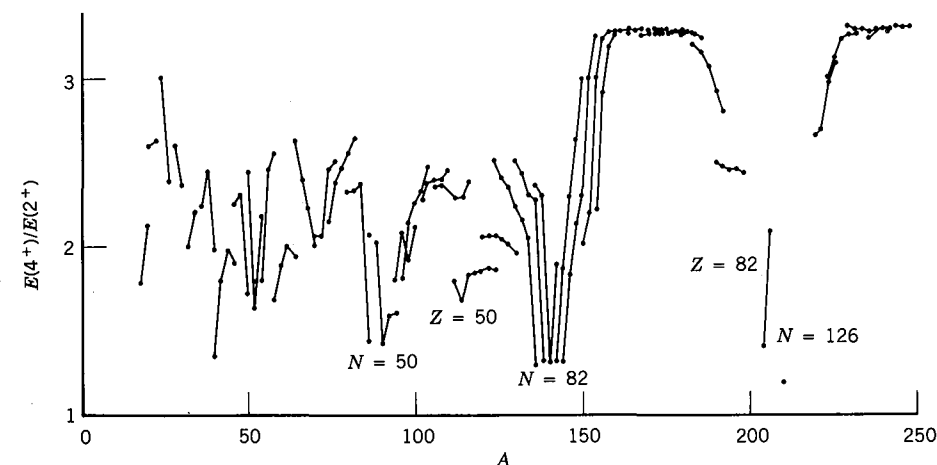


Figure 5.15b The ratio $E(4^+)/E(2^+)$ for the lowest 2^+ and 4^+ states of even- Z , even- N nuclei. The lines connect sequences of isotopes.

is roughly 2.0 for nuclei below $A = 150$ and very constant at 3.3 for $150 < A < 190$ and $A > 230$. The magnetic moments of the 2^+ states (Figure 5.16a) are fairly constant in the range 0.7–1.0, and the electric quadrupole moments (Figure 5.16b) are small for $A < 150$ and much larger for $A > 150$. These illustrations suggest that we must consider two types of collective structure, for the nuclei with $A < 150$ seem to show one set of properties and the nuclei with $150 < A < 190$ show quite a different set.

The nuclei with $A < 150$ are generally treated in terms of a model based on vibrations about a spherical equilibrium shape, while nuclei with A between 150 and 190 show structures most characteristic of rotations of a nonspherical system. Vibrations and rotations are the two major types of collective nuclear

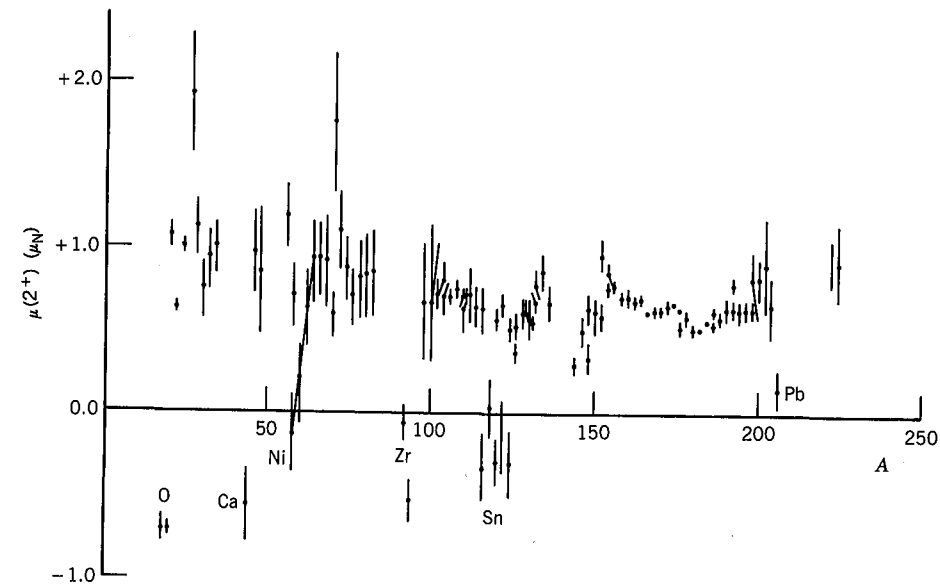


Figure 5.16a Magnetic moments of lowest 2^+ states of even-Z, even-N nuclei. Shell-model nuclei showing noncollective behavior are indicated.

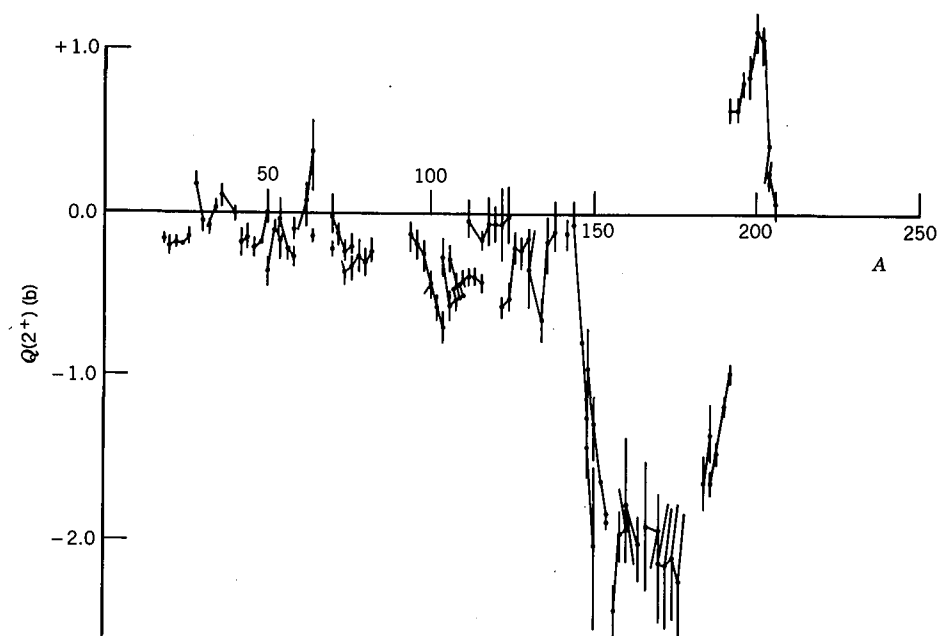


Figure 5.16b Electric quadrupole moments of lowest 2^+ states of even-Z, even-N nuclei. The lines connect sequences of isotopes.

motion, and we will consider each in turn. The collective nuclear model is often called the “liquid drop” model, for the vibrations and rotations of a nucleus resemble those of a suspended drop of liquid and can be treated with a similar mathematical analysis.

Nuclear Vibrations

Imagining a liquid drop vibrating at high frequency, we can get a good idea of the physics of nuclear vibrations. Although the average shape is spherical, the instantaneous shape is not. It is convenient to give the instantaneous coordinate $R(t)$ of a point on the nuclear surface at (θ, ϕ) , as shown in Figure 5.17, in terms of the spherical harmonics $Y_{\lambda\mu}(\theta, \phi)$. Each spherical harmonic component will have an amplitude $\alpha_{\lambda\mu}(t)$:

$$R(t) = R_{av} + \sum_{\lambda \geq 1} \sum_{\mu = -\lambda}^{+\lambda} \alpha_{\lambda\mu}(t) Y_{\lambda\mu}(\theta, \phi) \quad (5.13)$$

The $\alpha_{\lambda\mu}$ are not completely arbitrary; reflection symmetry requires that $\alpha_{\lambda\mu} = \alpha_{\lambda, -\mu}$, and if we assume the nuclear fluid to be incompressible, further restrictions apply. The constant ($\lambda = 0$) term is incorporated into the average radius R_{av} , which is just $R_0 A^{1/3}$. A typical $\lambda = 1$ vibration, known as a *dipole* vibration, is shown in Figure 5.18. Notice that this gives a net displacement of the center of mass and therefore cannot result from the action of internal nuclear forces. We therefore consider the next lowest mode, the $\lambda = 2$ (quadrupole) vibration. In analogy with the quantum theory of electromagnetism, in which a unit of electromagnetic energy is called a photon, a quantum of vibrational energy is

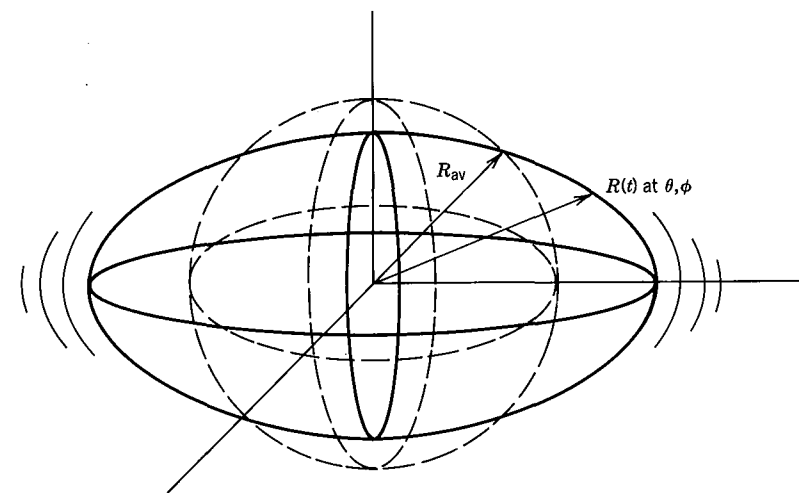


Figure 5.17 A vibrating nucleus with a spherical equilibrium shape. The time-dependent coordinate $R(t)$ locates a point on the surface in the direction θ, ϕ .

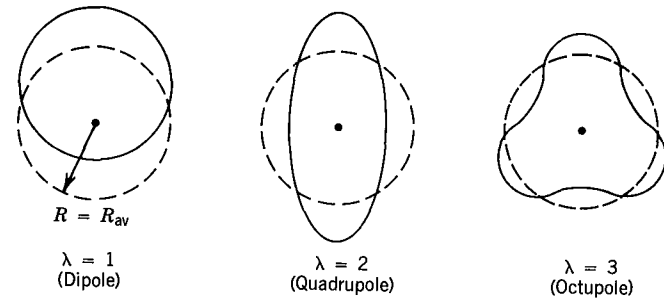


Figure 5.18 The lowest three vibrational modes of a nucleus. The drawings represent a slice through the midplane. The dashed lines show the spherical equilibrium shape and the solid lines show an instantaneous view of the vibrating surface.

called a *phonon*. Whenever we produce mechanical vibrations, we can equivalently say that we are producing vibrational phonons. A single unit of $\lambda = 2$ nuclear vibration is thus a *quadrupole phonon*.

Let's consider the effect of adding one unit of vibrational energy (a quadrupole phonon) to the 0^+ ground state of an even-even nucleus. The $\lambda = 2$ phonon carries 2 units of angular momentum (it adds a $Y_{2\mu}$ dependence to the nuclear wave function, just like a $Y_{\ell m}$ with $\ell = 2$) and even parity, since the parity of a $Y_{\ell m}$ is $(-1)^\ell$. Adding two units of angular momentum to a 0^+ state gives only a 2^+ state, in exact agreement with the observed spin-parity of first excited states of spherical even- Z , even- N nuclei. (The energy of the quadrupole phonon is not predicted by this theory and must be regarded as an adjustable parameter.) Suppose now we add a second quadrupole phonon. There are 5 possible components μ for each phonon and therefore 25 possible combinations of the $\lambda\mu$ for the two phonons, as enumerated in Table 5.2. Let's try to examine the resulting sums. There is one possible combination with total $\mu = +4$. It is natural to associate this with a transfer of 4 units of angular momentum (a $Y_{\ell m}$ with $m = +4$ and therefore $\ell = 4$). There are two combinations with total $\mu = +3$: ($\mu_1 = +1, \mu_2 = +2$) and ($\mu_1 = +2, \mu_2 = +1$). However, when we make the proper symmetric combination of the phonon wave functions (phonons, with integer spins, must have symmetric total wave functions; see Section 2.7), only

Table 5.2 Combinations of z Projections of Two Quadrupole Phonons into a Resultant Total z Component^a

μ_2	μ_1				
	-2	-1	0	+1	+2
-2	-4	-3	-2	-1	0
-1	-3	-2	-1	0	+1
0	-2	-1	0	+1	+2
+1	-1	0	+1	+2	+3
+2	0	+1	+2	+3	+4

^aThe entries show $\mu = \mu_1 + \mu_2$.

one combination appears. There are three combinations that give $\mu = +2$: (μ_1, μ_2) = $(+2, 0)$, $(+1, +1)$, and $(0, +2)$. The first and third must be combined into a symmetric wave function; the $(+1, +1)$ combination is already symmetric. Continuing in this way, we would find not 25 but 15 possible allowed combinations: one with $\mu = +4$, one with $\mu = +3$, two with $\mu = +2$, two with $\mu = +1$, three with $\mu = 0$, two with $\mu = -1$, two with $\mu = -2$, one with $\mu = -3$ and one with $\mu = -4$. We can group these in the following way:

$$\ell = 4 \quad \mu = +4, +3, +2, +1, 0, -1, -2, -3, -4$$

$$\ell = 2 \quad \mu = +2, +1, 0, -1, -2$$

$$\ell = 0 \quad \mu = 0$$

Thus we expect a triplet of states with spins $0^+, 2^+, 4^+$ at twice the energy of the first 2^+ state (since two identical phonons carry twice as much energy as one). This $0^+, 2^+, 4^+$ triplet is a common feature of vibrational nuclei and gives strong support to this model. The three states are never exactly at the same energy, owing to additional effects not considered in this simple model. A similar calculation for three quadrupole phonons gives states $0^+, 2^+, 3^+, 4^+, 6^+$ (see Problem 10).

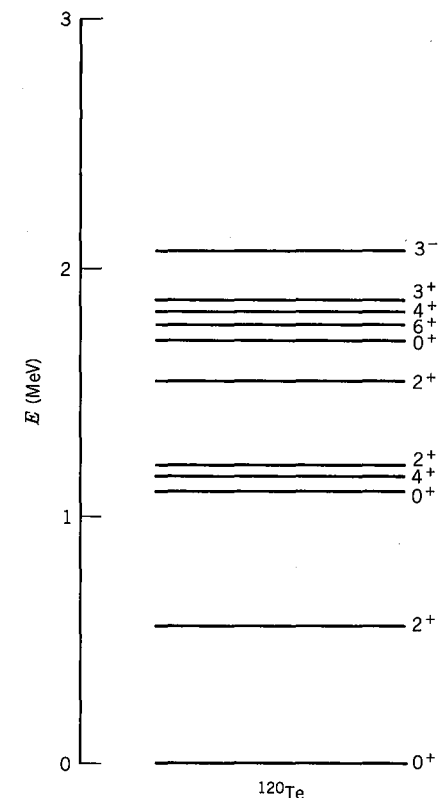


Figure 5.19 The low-lying levels of ^{120}Te . The single quadrupole phonon state (first 2^+), the two-phonon triplet, and the three-phonon quintuplet are obviously seen. The 3^- state presumably is due to the octupole vibration. Above 2 MeV the structure becomes quite complicated, and no vibrational patterns can be seen.

The next highest mode of vibration is the $\lambda = 3$ *octupole* mode, which carries three units of angular momentum and negative parity. Adding a single octupole phonon to the 0^+ ground state gives a 3^- state. Such states are also commonly found in vibrational nuclei, usually at energies somewhat above the two-phonon triplet. As we go higher in energy, the vibrational structure begins to give way to particle excitation corresponding to the breaking of a pair in the ground state. These excitations are very complicated to handle and are not a part of the collective structure of nuclei.

The vibrational model makes several predictions that can be tested in the laboratory. If the equilibrium shape is spherical, the quadrupole moments of the first 2^+ state should vanish; Figure 5.16*b* showed they are small and often vanishing in the region $A < 150$. The magnetic moments of the first 2^+ states are predicted to be $2(Z/A)$, which is in the range 0.8–1.0 for the nuclei considered; this is also in reasonable agreement with experiment. The predicted ratio $E(4^+)/E(2^+)$ is 2.0, if the 4^+ state is a member of the two-phonon triplet and the 2^+ state is the first excited state; Figure 5.15*b* shows reasonable agreement with this prediction in the range $A < 150$. In Chapter 10 we show the good agreement with γ -ray transition probabilities as well. Figure 5.19 shows an example of the low-lying level structure of a typical “vibrational” nucleus, and many of the predicted features are readily apparent. Thus the spherical vibrational model gives us quite an accurate picture of the structure of these nuclei.

Nuclear Rotations

Rotational motion can be observed only in nuclei with nonspherical equilibrium shapes. These nuclei can have substantial distortions from spherical shape and are often called *deformed nuclei*. They are found in the mass ranges $150 < A < 190$ and $A > 220$ (rare earths and actinides). Figure 5.10 showed that the odd-mass nuclei in these regions also have quadrupole moments that are unexpectedly large. A common representation of the shape of these nuclei is that of an ellipsoid of revolution (Figure 5.20), the surface of which is described by

$$R(\theta, \phi) = R_{av} [1 + \beta Y_{20}(\theta, \phi)] \quad (5.14)$$

which is independent of ϕ and therefore gives the nucleus cylindrical symmetry. The *deformation parameter* β is related to the eccentricity of the ellipse as

$$\beta = \frac{4}{3} \sqrt{\frac{\pi}{5}} \frac{\Delta R}{R_{av}} \quad (5.15)$$

where ΔR is the difference between the semimajor and semiminor axes of the ellipse. It is customary (although not quite exact) to take $R_{av} = R_0 A^{1/3}$. The approximation is not exact because the volume of the nucleus described by Equation 5.14 is not quite $\frac{4}{3}\pi R_{av}^3$; see Problem 11. The axis of symmetry of Equation 5.14 is the reference axis relative to which θ is defined. When $\beta > 0$, the nucleus has the elongated form of a *prolate* ellipsoid; when $\beta < 0$, the nucleus has the flattened form of an *oblate* ellipsoid.

One indicator of the stable deformation of a nucleus is a large electric quadrupole moment, such as those shown in Figure 5.10. The relationship

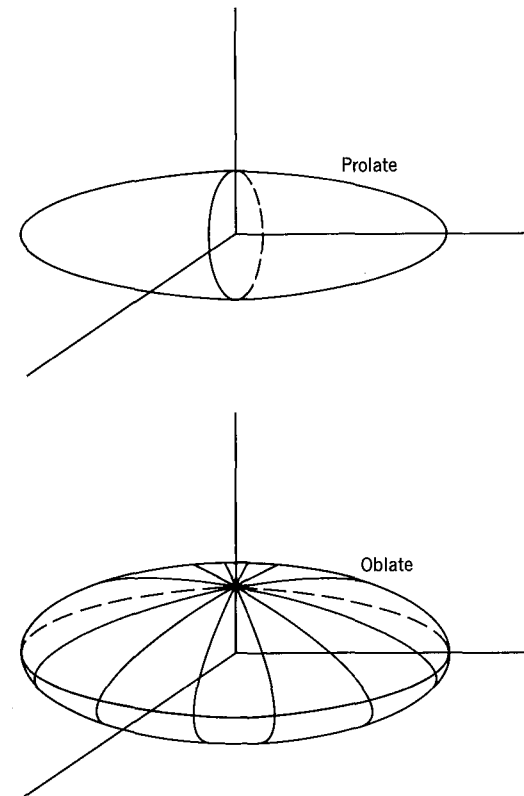


Figure 5.20 Equilibrium shapes of nuclei with permanent deformations. These sketches differ from Figures 5.17 and 5.18 in that these do not represent snapshots of a moving surface at a particular instant of time, but instead show the static shape of the nucleus.

between the deformation parameter and the quadrupole moment is

$$Q_0 = \frac{3}{\sqrt{5\pi}} R_{av}^2 Z \beta (1 + 0.16\beta) \quad (5.16)$$

The quadrupole moment Q_0 is known as the *intrinsic* quadrupole moment and would only be observed in a frame of reference in which the nucleus were at rest. In the laboratory frame of reference, the nucleus is rotating and quite a different quadrupole moment Q is measured. In fact, as indicated in Figure 5.21, rotating a prolate intrinsic distribution about an axis perpendicular to the symmetry axis (no rotations can be observed parallel to the symmetry axis) gives a time-averaged oblate distribution. Thus for $Q_0 > 0$, we would observe $Q < 0$. The relationship between Q and Q_0 depends on the nuclear angular momentum; for 2^+ states, $Q = -\frac{2}{7}Q_0$. Figure 5.16*b* shows $Q \approx -2b$ for nuclei in the region of stable permanent deformations ($150 \leq A \leq 190$), and so $Q_0 \approx +7b$. From Equation 5.16, we would deduce $\beta \approx 0.29$. This corresponds to a substantial deviation from a spherical nucleus; the difference in the lengths of the semimajor and semiminor axes is, according to Equation 5.15, about 0.3 of the nuclear radius.

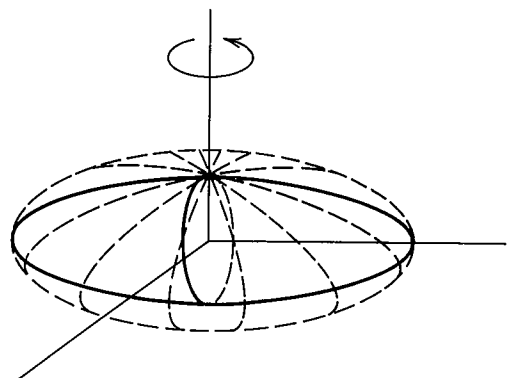


Figure 5.21 Rotating a static prolate distribution about an axis perpendicular to its symmetry axis gives in effect a smeared-out oblate (flattened) distribution.

The kinetic energy of a rotating object is $\frac{1}{2}\mathcal{I}\omega^2$, where \mathcal{I} is the moment of inertia. In terms of the angular momentum $\ell = \mathcal{I}\omega$, the energy is $\ell^2/2\mathcal{I}$. Taking the quantum mechanical value of ℓ^2 , and letting I represent the angular momentum quantum number, gives

$$E = \frac{\hbar^2}{2\mathcal{I}}I(I+1) \quad (5.17)$$

for the energies of a rotating object in quantum mechanics. Increasing the quantum number I corresponds to adding rotational energy to the nucleus, and the nuclear excited states form a sequence known as a *rotational band*. (Excited states in molecules also form rotational bands, corresponding to rotations of the molecule about its center of mass.) The ground state of an even- Z , even- N nucleus is always a 0^+ state, and the mirror symmetry of the nucleus restricts the sequence of rotational states in this special case to *even* values of I . We therefore expect to see the following sequence of states:

$$\begin{aligned} E(0^+) &= 0 \\ E(2^+) &= 6(\hbar^2/2\mathcal{I}) \\ E(4^+) &= 20(\hbar^2/2\mathcal{I}) \\ E(6^+) &= 42(\hbar^2/2\mathcal{I}) \\ E(8^+) &= 72(\hbar^2/2\mathcal{I}) \end{aligned}$$

and so on.

Figure 5.22 shows the excited states of a typical rotational nucleus. The first excited state is at $E(2^+) = 91.4$ keV, and thus we have $\hbar^2/2\mathcal{I} = 15.2$ keV. The energies of the next few states in the ground-state rotational band are computed to be

$$\begin{aligned} E(4^+) &= 20(\hbar^2/2\mathcal{I}) = 305 \text{ keV} && \text{(measured 300 keV)} \\ E(6^+) &= 42(\hbar^2/2\mathcal{I}) = 640 \text{ keV} && \text{(measured 614 keV)} \\ E(8^+) &= 72(\hbar^2/2\mathcal{I}) = 1097 \text{ keV} && \text{(measured 1025 keV)} \end{aligned}$$

The calculated energy levels are not quite exact (perhaps because the nucleus behaves somewhat like a fluid of nucleons and not quite like a rigid object with a fixed moment of inertia), but are good enough to give us confidence that we have at least a rough idea of the origin of the excited levels. In particular, the predicted

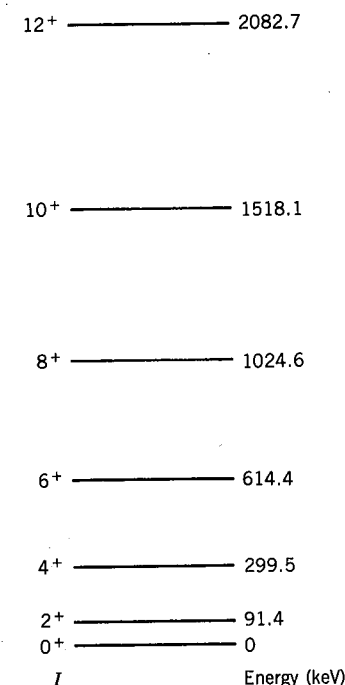


Figure 5.22 The excited states resulting from rotation of the ground state in ^{164}Er .

ratio $E(4^+)/E(2^+)$ is 3.33, in remarkable agreement with the systematics of nuclear levels for $150 < A < 190$ and $A > 230$ shown in Figure 5.15b.

We can gain some insight into the structure of deformed nuclei by considering the moment of inertia in two extreme cases. A solid ellipsoid of revolution of mass M whose surface is described by Equation 5.14 has a rigid moment of inertia

$$\mathcal{I}_{\text{rigid}} = \frac{2}{5}MR_{\text{av}}^2(1 + 0.31\beta) \quad (5.18)$$

which of course reduces to the familiar value for a sphere when $\beta = 0$. For a typical nucleus in the deformed region ($A \approx 170$), this gives a rotational energy constant

$$\frac{\hbar^2}{2\mathcal{I}_{\text{rigid}}} \cong 6 \text{ keV}$$

which is of the right order of magnitude but is too small compared with the observed values (about 15 keV for $E(2^+) = 90$ keV). That is, the rigid moment of inertia is too large by about a factor of 2–3. We can take the other extreme and regard the nucleus as a fluid inside a rotating ellipsoidal vessel, which would give a moment of inertia

$$\mathcal{I}_{\text{fluid}} = \frac{9}{8\pi}MR_{\text{av}}^2\beta \quad (5.19)$$

from which we would estimate

$$\frac{\hbar^2}{2\mathcal{I}_{\text{fluid}}} \cong 90 \text{ keV}$$

The fluid moment inertia is thus too small, and we conclude $\mathcal{I}_{\text{rigid}} > \mathcal{I} > \mathcal{I}_{\text{fluid}}$. The rotational behavior is thus intermediate between a rigid object, in which the particles are tightly bonded together, and a fluid, in which the particles are only weakly bonded. (We probably should have guessed this result, based on our studies of the nuclear force. Strong forces exist between a nucleon and its immediate neighbors only, and thus a nucleus does not show the long-range structure that would characterize a rigid solid.)

Another indication of the lack of rigidity of the nucleus is the increase in the moment of inertia that occurs at high angular momentum or rotational frequency. This effect, called "centrifugal stretching," is seen most often in heavy-ion reactions, to be discussed in Section 11.13.

Of course, the nucleus has no "vessel" to define the shape of the rotating fluid; it is the potential supplied by the nucleons themselves which gives the nucleus its shape. The next issue to be faced is whether the concept of a shape has any meaning for a rotating nucleus. If the rotation is very fast compared with the speed of nucleons in their "orbits" defined by the nuclear potential (as seen in a frame of reference in which the nucleus is at rest), then the concept of a static nuclear shape is not very meaningful because the motion of the nucleons will be dominated by the rotation. The average kinetic energy of a nucleon in a nucleus is of the order of 20 MeV, corresponding to a speed of approximately $0.2c$. This is a reasonable estimate for the speed of internal motion of the nucleons. The angular velocity of a rotating state is $\omega = \sqrt{2E/\mathcal{I}}$, where E is the energy of the state. For the first rotational state, $\omega \approx 1.1 \times 10^{20}$ rad/s and a nucleon near the surface would rotate with a tangential speed of $v \approx 0.002c$. The rotational motion is therefore far slower than the internal motion. The correct picture of a rotating deformed nucleus is therefore a stable equilibrium shape determined by nucleons in rapid internal motion in the nuclear potential, with the entire resulting distribution rotating sufficiently slowly that the rotation has little effect on the nuclear structure or on the nucleon orbits. (The rotational model is sometimes described as "adiabatic" for this reason.)

It is also possible to form other kinds of excited states upon which new rotational bands can be built. Examples of such states, known as *intrinsic states* because they change the intrinsic structure of the nucleus, are vibrational states (in which the nucleus vibrates about a deformed equilibrium shape) and pair-breaking particle excitations. If the intrinsic state has spin different from zero, the rotational band built on that state will have the sequence of spins $I, I + 1, I + 2, \dots$. The vibrational states in deformed nuclei are of two types: β vibrations, in which the deformation parameter β oscillates and the nucleus preserves its cylindrical symmetry, and γ vibrations, in which the cylindrical symmetry is violated. (Picture a nucleus shaped like a football. β vibrations correspond to pushing and pulling on the ends of the football, while γ vibrations correspond to pushing and pulling on its sides.) Both the vibrational states and the particle excitations occur at energies of about 1 MeV, while the rotational spacing is much smaller (typically $\hbar^2/2\mathcal{I} \approx 10\text{--}20$ keV).

Figure 5.23 shows the complete low-energy structure of ^{164}Er . Although the entire set of excited states shows no obvious patterns, knowing the spin-parity assignments helps us to group the states into rotational bands, which show the characteristic $I(I + 1)$ spacing. Other properties of the excited states (for example, γ -ray emission probabilities) also help us to identify the structure.

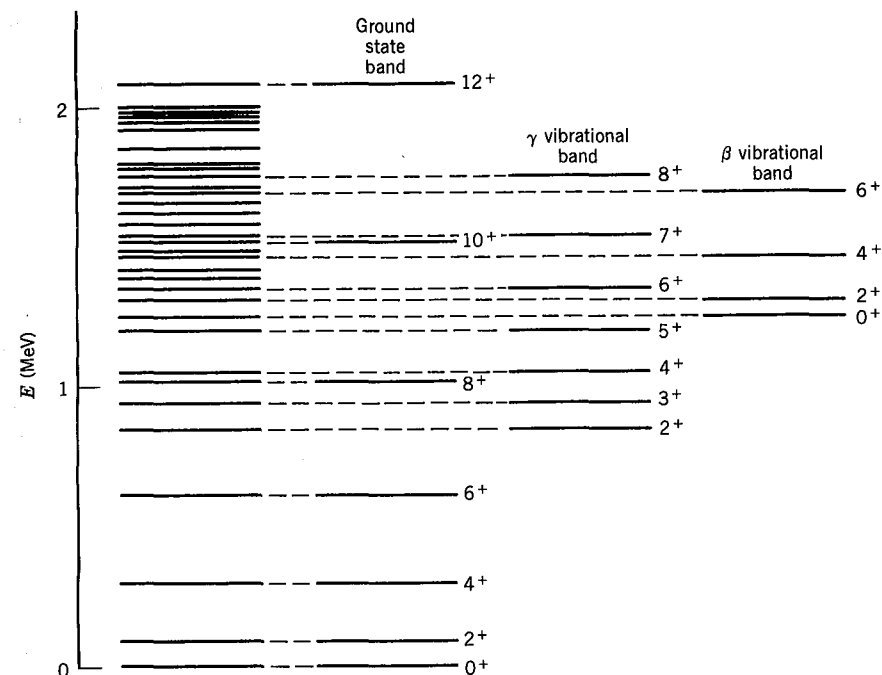


Figure 5.23 The states of ^{164}Er below 2 MeV. Most of the states are identified with three rotational bands: one built on the deformed ground state, a second built on a γ -type vibration (in which the surface vibrates transverse to the symmetry axis), and a third built on a β -type vibration (in which the surface vibrates along the symmetry axis). Many of the other excited states originate from pair-breaking particle excitations and their associated rotational bands.

Both the vibrational and rotational collective motions give the nucleus a magnetic moment. We can regard the movement of the protons as an electric current, and a single proton moving with angular momentum quantum number ℓ would give a magnetic moment $\mu = \ell\mu_N$. However, the entire angular momentum of a nuclear state does not arise from the protons alone; the neutrons also contribute, and if we assume that the protons and neutrons move with identical collective motions (a reasonable but not quite exact assumption), we would predict that the protons contribute to the total nuclear angular momentum a fraction of nearly Z/A . (We assume that the collective motion of the neutrons does not contribute to the magnetic moment, and we also assume that the protons and neutrons are all coupled pairwise so that the spin magnetic moments do not contribute.) The collective model thus predicts for the magnetic moment of a vibrational or rotational state of angular momentum I

$$\mu(I) = I \frac{Z}{A} \mu_N \quad (5.20)$$

For light nuclei, $Z/A \approx 0.5$ and $\mu(2) \approx +1\mu_N$, while for heavier nuclei, $Z/A \approx 0.4$ and $\mu(2) \approx +0.8\mu_N$. Figure 5.16a shows that, with the exception of closed-shell nuclei (for which the collective model is not valid), the magnetic moments of the 2^+ states are in very good agreement with this prediction.

As a final point in this brief introduction to nuclear collective motion, we must try to justify the origin of collective behavior based on a more microscopic approach to nuclear structure. This is especially true for rotational nuclei with permanent deformations. We have already seen how well the shell model with a spherically symmetric potential works for many nuclei. We can easily allow the shell-model potential to vibrate about equilibrium when energy is added to the nucleus, and so the vibrational motion can be handled in a natural way in the shell model. As we learned in our discussion of the ^{130}Sn structure at the beginning of this section, we can analyze the collective vibrational structure from an even more microscopic approach; for example, we consider all valence nucleons (those outside closed shells), find all possible couplings (including those that break pairs) giving 2^+ resultant spins, and try to find the correct mixture of wave functions that gives the observed 2^+ first excited state. If there are many possible couplings, this procedure may turn out to be mathematically complex, but the essentials of the shell model on which it is based are not significantly different from the extreme independent particle model we considered in the previous section. This approach works for spherical nuclei, but it does not lead naturally to a rotational nucleus with a permanent deformation.

Here is the critical question: How do shell-model orbits, calculated using a spherical potential, result in a nonspherical nucleus? We get a clue to the answer to this question by superimposing a diagram showing the "magic numbers" on a

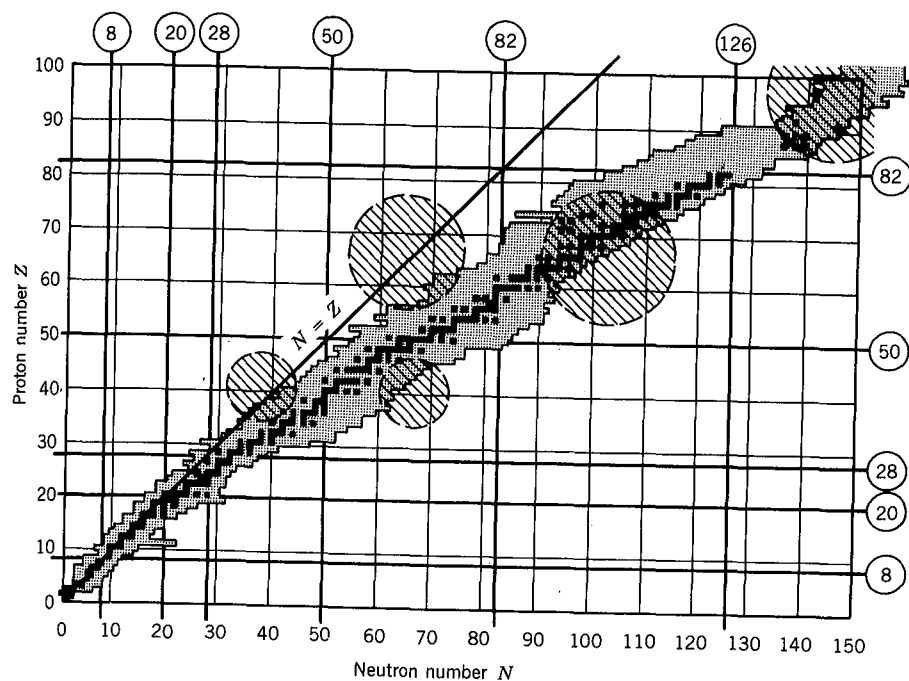


Figure 5.24 The crosshatched areas show the regions far from closed shells where we expect that the cooperative effects of many single-particle shell-model states may combine to produce a permanent nuclear deformation. Such deformed nuclei have been identified in all of the regions where the crosshatched areas overlap the known nuclei.

chart of the known nuclear species, as shown in Figure 5.24. The deformed nuclei exist only in regions far from filled neutron and proton shells. Just as the cooperative effect of a few nucleon pairs outside of a filled shell was responsible for the microscopic structure of the vibrations of spherical nuclei, the cooperative effect of many valence nucleon pairs can distort the "core" of nucleons until the equilibrium shape becomes strongly deformed.

5.3 MORE REALISTIC NUCLEAR MODELS

Both the shell model for odd- A nuclei and the collective model for even-even nuclei are idealizations that are only approximately valid for real nuclei, which are far more complex in their structure than our simple models suggest. Moreover, in real nuclei we cannot "turn off" one type of structure and consider only the other. Thus even very collective nuclei show single-particle effects, while the core of nucleons in shell-model nuclei may contribute collective effects that we have ignored up to this point. The structure of most nuclei cannot be quite so neatly divided between single-particle and collective motion, and usually we must consider a combination of both. Such a *unified nuclear model* is mathematically too complicated to be discussed here, and hence we will merely illustrate a few of the resulting properties of nuclei and try to relate them to the more elementary aspects of the shell and collective models.

Many-Particle Shell Model

In our study of the shell model, we considered only the effects due to the last unpaired single particle. A more realistic approach for odd- A nuclei would be to include all particles outside of closed shells. Let us consider for example the nuclei with odd Z or N between 20 and 28, so that the odd nucleons are in the $f_{7/2}$ shell. For simplicity, we shall confine our discussion to one kind of nucleon only, and thus we require not only that there be an even number of the other kind of nucleon, but also that it be a magic number. Figure 5.25 shows the lower excited states of several such nuclei. The nuclei whose structure is determined by a *single* particle (^{41}Ca and ^{55}Co) show the expected levels—a $\frac{7}{2}^-$ ground state, corresponding to the single odd $f_{7/2}$ particle (or vacancy, in the case of ^{55}Co , since a single vacancy or hole in a shell behaves like a single particle in the shell), and a $\frac{3}{2}^-$ excited state at about 2 MeV, corresponding to exciting the single odd particle to the $p_{3/2}$ state. The nuclei with 3 or 5 particles in the $f_{7/2}$ level show a much richer spectrum of states, and in particular the very low negative-parity states cannot be explained by the extreme single-particle shell model. If the $\frac{5}{2}^-$ state, for instance, originated from the excitation of a single particle to the $f_{5/2}$ shell, we would expect it to appear above 2 MeV because the $f_{5/2}$ level occurs above the $p_{3/2}$ level (see Figure 5.6); the lowest $\frac{5}{2}^-$ level in the single-particle nuclei occurs at 2.6 MeV (in ^{41}Ca) and 3.3 MeV (in ^{55}Co).

We use the shorthand notation $(f_{7/2})^n$ to indicate the configuration with n particles in the $f_{7/2}$ shell, and we consider the possible resultant values of I for the configuration $(f_{7/2})^3$. (From the symmetry between particles and holes, the levels of three holes, or five particles, in the $f_{7/2}$ shell will be the same.) Because

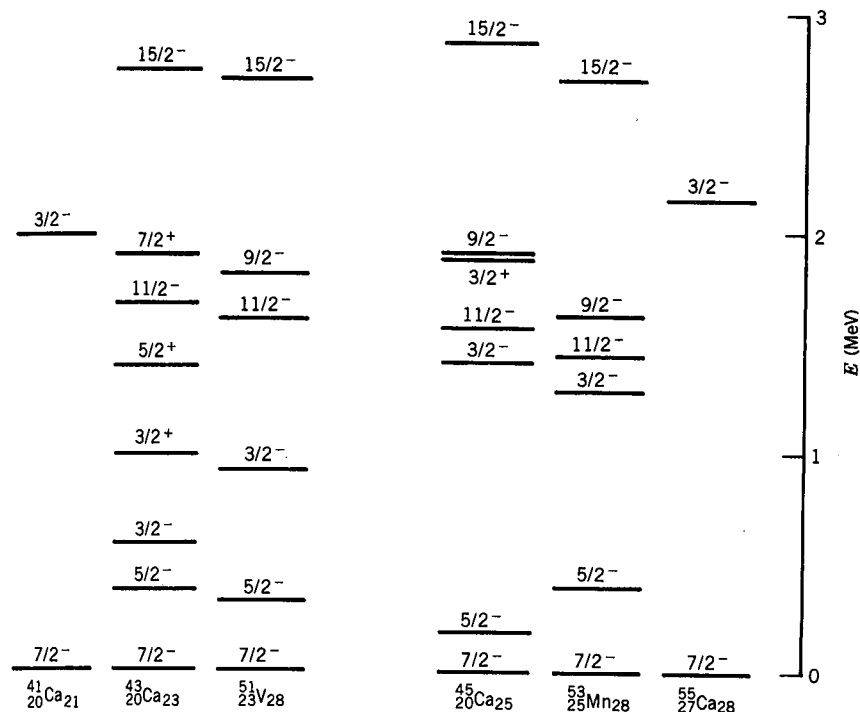


Figure 5.25 Excited states of some nuclei with valence particles in the $f_{7/2}$ shell. All known levels below about 2 MeV are shown, and in addition the $\frac{15}{2}^-$ state is included.

the nucleons have half-integral spins, they must obey the Pauli principle, and thus no two particles can have the same set of quantum numbers. Each particle in the shell model is described by the angular momentum $j = \frac{7}{2}$, which can have the projections or z components corresponding to $m = \pm \frac{1}{2}, \pm \frac{3}{2}, \pm \frac{5}{2}, \pm \frac{7}{2}$. The Pauli principle requires that each of the 3 particles have a different value of m . Immediately we conclude that the maximum value of the total projection, $M = m_1 + m_2 + m_3$, for the three particles is $+\frac{7}{2} + \frac{5}{2} + \frac{3}{2} = +\frac{15}{2}$. (Without the Pauli principle, the maximum would be $\frac{21}{2}$.) We therefore expect to find no state in the configuration $(f_{7/2})^3$ with I greater than $\frac{15}{2}$; the maximum resultant angular momentum is $I = \frac{15}{2}$, which can have all possible M from $+\frac{15}{2}$ to $-\frac{15}{2}$. The next highest possible M is $\frac{13}{2}$, which can only be obtained from $+\frac{7}{2} + \frac{5}{2} + \frac{1}{2}$ ($+\frac{7}{2} + \frac{3}{2} + \frac{3}{2}$ is not permitted, nor is $+\frac{7}{2} + \frac{7}{2} - \frac{1}{2}$). This single $M = \frac{13}{2}$ state must belong to the M states we have already assigned to the $I = \frac{15}{2}$ configuration; thus we have no possibility to have a $I = \frac{13}{2}$ resultant. Continuing in this way, we find two possibilities to obtain $M = +\frac{11}{2}$ ($+\frac{7}{2} + \frac{3}{2} + \frac{1}{2}$ and $+\frac{7}{2} + \frac{5}{2} - \frac{1}{2}$); there are thus two possible $M = +\frac{11}{2}$ states, one for the $I = \frac{15}{2}$ configuration and another that we can assign to $I = \frac{11}{2}$. Extending this reasoning, we expect to find the following states for $(f_{7/2})^3$ or $(f_{7/2})^5$: $I = \frac{15}{2}, \frac{11}{2}, \frac{9}{2}, \frac{7}{2}, \frac{5}{2}$, and $\frac{3}{2}$. Because each of the three or five particles has negative parity, the resultant parity is $(-1)^3$. The nuclei shown in Figure 5.25 show low-lying negative-parity states with the expected spins (and also with the expected absences—no low-lying $\frac{1}{2}^-$ or $\frac{3}{2}^-$ states appear).

Although this analysis is reasonably successful, it is incomplete—if we do indeed treat all valence particles as independent and equivalent, then the energy of a level should be independent of the orientation of the different m 's—that is, all of the resultant I 's should have the same energy. This is obviously not even approximately true; in the case of the $(f_{7/2})^3$ multiplet, the energy splitting between the highest and lowest energy levels is 2.7 MeV, about the same energy as pair-breaking and particle-exciting interactions. We can analyze these energy splittings in terms of a *residual interaction* between the valence particles, and thus the level structure of these nuclei gives us in effect a way to probe the nucleon-nucleon interaction in an environment different from the free-nucleon studies we discussed in Chapter 4.

As a final comment, we state without proof that the configurations with n particles in the same shell have another common feature that lends itself to experimental test—their magnetic moments should all be proportional to I . That is, given two different states 1 and 2 belonging to the same configuration, we expect

$$\frac{\mu_1}{\mu_2} = \frac{I_1}{I_2} \quad (5.21)$$

Unfortunately, few of the excited-state magnetic moments are well enough known to test this prediction. In the case of ^{51}V , the ground-state moment is $\mu = +5.1514 \pm 0.0001 \mu_N$ and the moment of the first excited state is $\mu = +3.86 \pm 0.33 \mu_N$. The ratio of the moments is thus 1.33 ± 0.11 , in agreement with the expected ratio $\frac{7/2}{5/2} = 1.4$. In the case of ^{53}Mn , the ratio of moments of the same states is $5.024 \pm 0.007 \mu_N / 3.25 \pm 0.30 \mu_N = 1.55 \pm 0.14$. The evidence from the magnetic moments thus supports our assumption about the nature of these states.

Single-Particle States in Deformed Nuclei

The calculated levels of the nuclear shell model are based on the assumption that the nuclear potential is spherical. We know, however, that this is not true for nuclei in the range $150 \leq A \leq 190$ and $A > 230$. For these nuclei we should use a shell-model potential that approximates the actual nuclear shape, specifically a rotational ellipsoid. In calculations using the Schrödinger equation with a non-spherical potential, the angular momentum ℓ is no longer a “good” quantum number; that is, we cannot identify states by their spectroscopic notation (s, p, d, f , etc.) as we did for the spherical shell model. To put it another way, the states that result from the calculation have mixtures of different ℓ values (but based on consideration of parity, we expect mixtures of only even or only odd ℓ values).

In the spherical case, the energy levels of each single particle state have a degeneracy of $(2j + 1)$. (That is, relative to any arbitrary axis of our choice, all $2j + 1$ possible orientations of j are equivalent.) If the potential has a deformed shape, this will no longer be true—the energy levels in the deformed potential depend on the spatial orientation of the orbit. More precisely, the energy depends on the component of j along the symmetry axis of the core. For example, an $f_{7/2}$

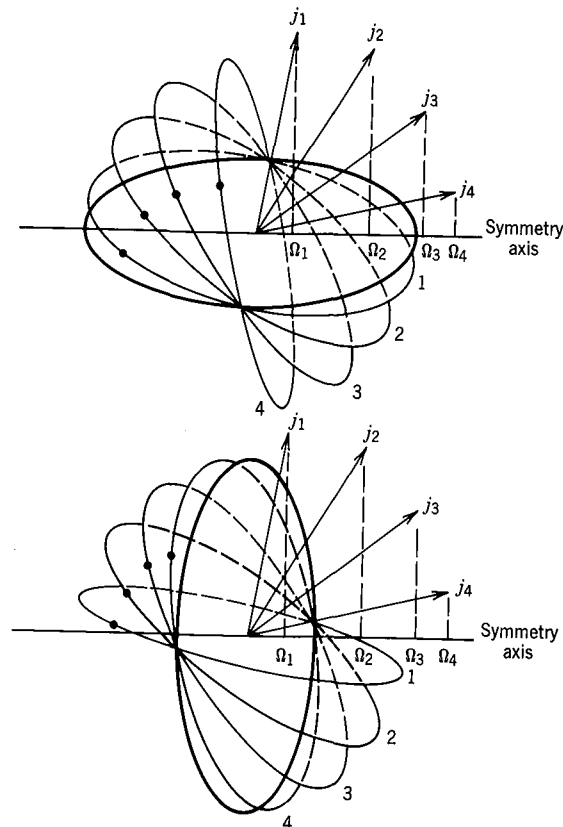


Figure 5.26 Single-particle orbits with $j = \frac{7}{2}$ and their possible projections along the symmetry axis, for prolate (top) and oblate (bottom) deformations. The possible projections are $\Omega_1 = \frac{1}{2}$, $\Omega_2 = \frac{3}{2}$, $\Omega_3 = \frac{5}{2}$, and $\Omega_4 = \frac{7}{2}$. (For clarity, only the positive projections are shown.) Note that in the prolate case, orbit 1 lies closest (on the average) to the core and will interact most strongly with the core; in the oblate case, it is orbit 4 that has the strongest interaction with the core.

nucleon can have eight possible components of j , ranging from $-\frac{7}{2}$ to $+\frac{7}{2}$. This component of j along the symmetry axis is generally denoted by Ω . Because the nuclei have reflection symmetry for either of the two possible directions of the symmetry axis, the components $+\Omega$ and $-\Omega$ will have the same energy, giving the levels a degeneracy of 2. That is, what we previously called the $f_{7/2}$ state splits up into four states if we deform the central potential; these states are labeled $\Omega = \frac{1}{2}, \frac{3}{2}, \frac{5}{2}, \frac{7}{2}$ and all have negative parity. Figure 5.26 indicates the different possible "orbits" of the odd particle for prolate and oblate deformations. For prolate deformations, the orbit with the smallest possible Ω (equal to $\frac{1}{2}$) interacts most strongly with the core and is thus more tightly bound and lowest in energy. The situation is different for oblate deformations, in which the orbit with maximum Ω (equal to j) has the strongest interaction with the core and the lowest energy. Figure 5.27 shows how the $f_{7/2}$ states would split as the deformation is increased.

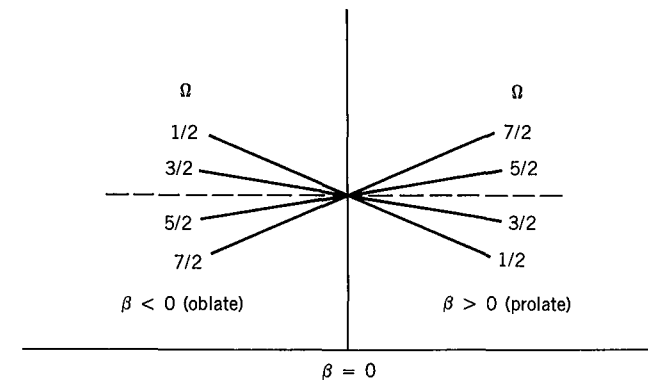


Figure 5.27 This shows directly the effect of the various orientations of the $f_{7/2}$ orbit. As shown in Figure 5.26, the orbit with component $\Omega = \frac{1}{2}$ along the symmetry axis has the strongest interaction with the *prolate* core and therefore lies lowest in energy. For an *oblate* core, it is the $\Omega = \frac{7}{2}$ component that lies lowest.

Of course, we must keep in mind that Figures 5.26 and 5.27 are not strictly correct because the spherical single-particle quantum numbers ℓ and j are not valid when the potential is deformed. The negative parity state with $\Omega = \frac{5}{2}$, for example, cannot be identified with the $f_{7/2}$ state, even though it approaches that state as $\beta \rightarrow 0$. The wave function of the $\Omega = \frac{5}{2}$ state can be expressed as a mixture (or linear combination) of many different ℓ and j (but only with $j \geq \frac{5}{2}$, in order to get a component of $\frac{5}{2}$). It is customary to make the approximation that states from different major oscillator shells (see Figures 5.4 and 5.6) do not mix. Thus, for example, the $\Omega = \frac{5}{2}$ state that approaches the $2f_{7/2}$ level as $\beta \rightarrow 0$ will include contributions from only those states of the 5th oscillator shell ($2f_{5/2}, 2f_{7/2}, 1h_{9/2}, 1h_{11/2}$). The 4th and 6th oscillator shells have the opposite parity and so will not mix, and the next odd-parity shells are far away and do not mix strongly. Writing the spherical wave functions as $\psi_{N\ell j}$, we must have

$$\psi'(\Omega) = \sum_{\ell j} a(N\ell j) \psi_{N\ell j} \quad (5.22)$$

where $\psi'(\Omega)$ represents the wave function of the deformed state Ω and where $a(N\ell j)$ are the expansion coefficients. For the $\Omega = \frac{5}{2}$ state

$$\psi'(\Omega) = a(53\frac{5}{2})\psi_{53\frac{5}{2}} + a(53\frac{7}{2})\psi_{53\frac{7}{2}} + a(55\frac{9}{2})\psi_{55\frac{9}{2}} + a(55\frac{11}{2})\psi_{55\frac{11}{2}} \quad (5.23)$$

The coefficients $a(N\ell j)$ can be obtained by solving the Schrödinger equation for the deformed potential, which was first done by S. G. Nilsson in 1955. The coefficients will vary with β , and of course for $\beta \rightarrow 0$ we expect $a(53\frac{7}{2})$ to approach 1 while the others all approach 0. For $\beta = 0.3$ (a typical prolate deformation), Nilsson calculated the values

$$\begin{aligned} a(53\frac{5}{2}) &= 0.267 & a(53\frac{7}{2}) &= 0.832 \\ a(55\frac{9}{2}) &= 0.415 & a(55\frac{11}{2}) &= -0.255 \end{aligned}$$

for the $\Omega = \frac{5}{2}$ level we have been considering.

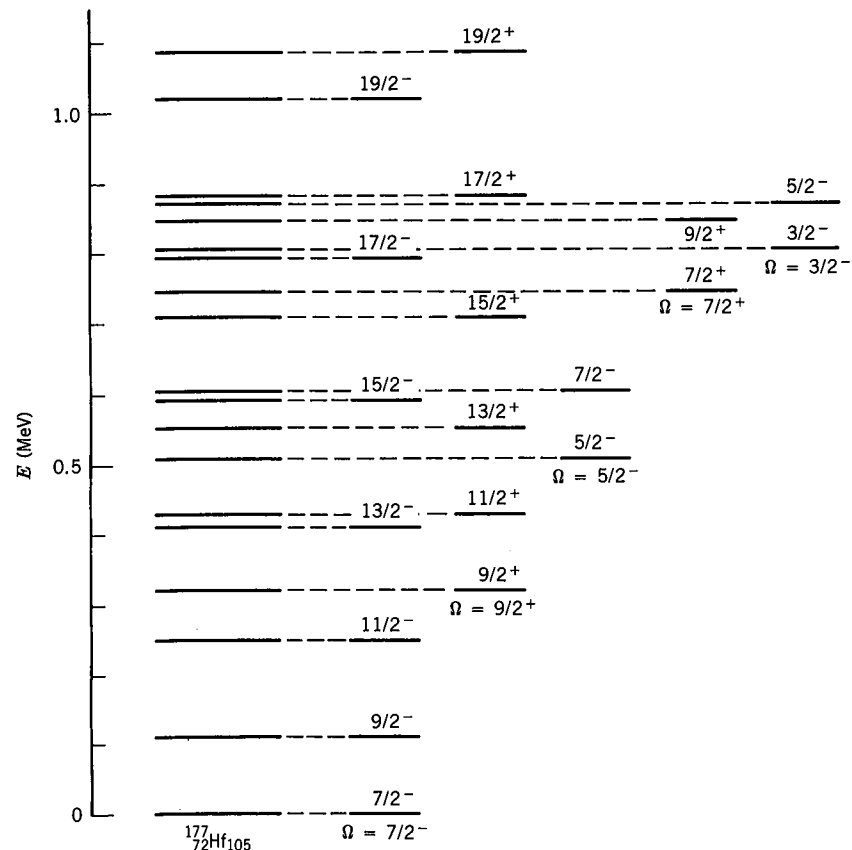


Figure 5.28 The energy levels of ^{177}Hf . As in the case of ^{164}Er (Figure 5.23), knowledge of the spin-parity assignments helps us to group the states into rotational bands. The lowest state in each band has $I = \Omega$, and the higher states follow the $I(I + 1)$ energy spacing.

Given such wave functions for single-particle states in deformed nuclei, we can then allow the nuclei to rotate, and we expect to find a sequence of rotational states, following the $I(I + 1)$ energy spacing, built on each single-particle state. The lowest state of the rotational band has $I = \Omega$, and as rotational energy is added the angular momentum increases in the sequence $I = \Omega, \Omega + 1, \Omega + 2, \dots$. Figure 5.28 shows the energy levels of the nucleus ^{177}Hf , in which two well-developed rotational bands have been found and several other single-particle states have been identified.

To interpret the observed single-particle levels, we require a diagram similar to Figure 5.27 but which shows all possible single-particle states and how their energies vary with deformation. Such a diagram is shown in Figure 5.29 for the neutron states that are appropriate to the $150 \leq A \leq 190$ region. Recalling that the degeneracy of each deformed single-particle level is 2, we proceed exactly as we did in the spherical shell model, placing two neutrons in each state up to $N = 105$ and two protons in each state up to $Z = 72$. We can invoke the pairing argument to neglect the single-particle states of the protons and examine the possible levels of the 105th neutron for the typical deformation of $\beta \approx 0.3$. You

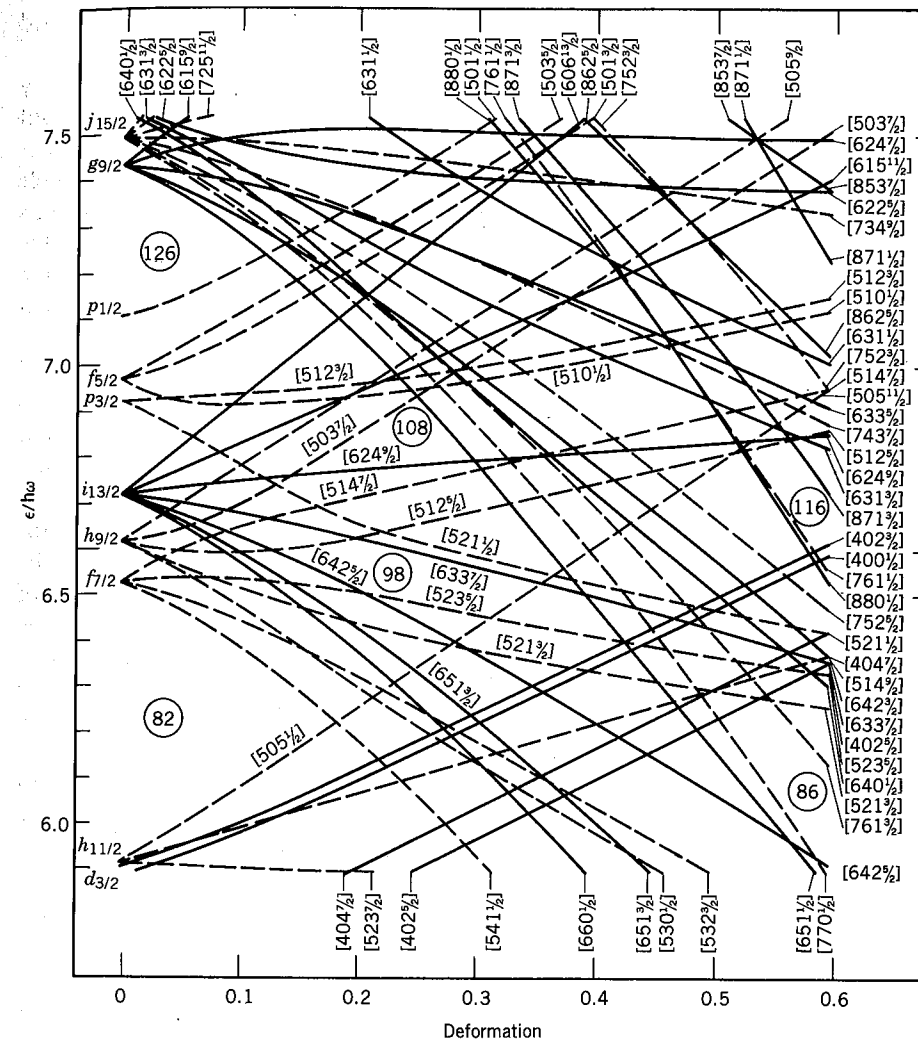


Figure 5.29 Energy levels for neutrons in a prolate deformed potential. The deformation is measured essentially by the parameter β . The numbers in the brackets label the states; for our purposes, we are interested only in the first number, which is the principal quantum number N of the oscillator shell and therefore tells us the parity of the state $(-1)^N$, and the last number, which is the component Ω . Solid lines show states with even parity, and dashed lines show odd parity. For a deformation between 0.2 and 0.3 (typical for nuclei in this region) the 105th neutron of ^{177}Hf would go into the state $[514 \frac{7}{2}]$, that is, an odd-parity state with $\Omega = \frac{7}{2}$. A small excitation takes it into the state $[624 \frac{9}{2}]$, an even parity state with $\Omega = \frac{9}{2}$. Both intrinsic states (and their associated rotational bands) can be seen in Figure 5.28. Other observed states in ^{177}Hf result from breaking a pair of neutrons in a lower state and exciting one to pair with the $\frac{7}{2}^-$ neutron. In this way, for instance, we could produce a single neutron in the state $[512 \frac{5}{2}]$, which gives the odd-parity $\Omega = \frac{5}{2}$ state in ^{177}Hf . From C. Gustafson et al., *Ark. Fys.* **36**, 613 (1967).

can see from the diagram that the expected single-particle levels correspond exactly with the observed levels of ^{177}Hf .

The general structure of the odd- A deformed nuclei is thus characterized by rotational bands built on single-particle states calculated from the deformed shell-model potential. The proton and neutron states are filled (two nucleons per state), and the nuclear properties are determined in the extreme single-particle limit by the properties of the odd particle. This model, with the wave functions calculated by Nilsson, has had extraordinary success in accounting for the nuclear properties in this region. In general, the calculations based on the properties of the odd particle have been far more successful in the deformed region than have the analogous calculations in the spherical region.

In this chapter we have discussed evidence for types of nuclear structure based on the *static* properties of nuclei—energy levels, spin-parity assignments, magnetic dipole and electric quadrupole moments. The wave functions that result from solving the Schrödinger equation for these various models permit many other features of nuclear structure to be calculated, particularly the transitions between different nuclear states. Often the evidence for collective structure, for instance, may be inconclusive based on the energy levels alone, while the transition probabilities between the excited states may give definitive proof of collective effects. It may also be the case that a specific excited state may have alternative interpretations—for example, a vibrational state or a 2-particle coupling. Studying the transition probabilities will usually help us to discriminate between these competing interpretations. The complete study of nuclear structure therefore requires that we study *radioactive decays*, which give spontaneous transitions between states, and *nuclear reactions*, in which the experimenter can select the initial and final states. In both cases, we can compare calculated decay and reaction probabilities with their experimental values in order to draw conclusions about the structure of nuclear states. The methods of each of these areas of *nuclear spectroscopy* will occupy us for most of the remainder of this text.

REFERENCES FOR ADDITIONAL READING

Nuclear physics texts providing more detailed and advanced information on nuclear models are the following: B. L. Cohen, *Concepts of Nuclear Physics* (New York: McGraw-Hill, 1971), Chapters 4–6; H. Frauenfelder and E. M. Henley, *Subatomic Physics* (Englewood Cliffs, NJ: Prentice-Hall, 1974), Chapters 14–16; M. A. Preston, *Physics of the Nucleus* (Reading, MA: Addison-Wesley, 1962), Chapters 7–10.

Two essential monographs, covering respectively the shell model and the collective model, have been written by recipients of the Nobel Prize for their work on nuclear models: M. G. Mayer and J. H. D. Jensen, *Elementary Theory of Nuclear Shell Structure* (New York: Wiley, 1955) and A. Bohr and B. R. Mottelson, *Nuclear Structure* (Reading, MA: Benjamin, 1975), Vol. 2 (Vol. 1 treats the shell model). Another comprehensive but advanced work is J. M. Eisenberg and W. Greiner, *Nuclear Models* (Amsterdam: North-Holland, 1970).

PROBLEMS

1. Give the expected shell-model spin and parity assignments for the ground states of (a) ^7Li ; (b) ^{11}B ; (c) ^{15}C ; (d) ^{17}F ; (e) ^{31}P ; (f) ^{141}Pr .
2. The low-lying levels of ^{13}C are ground state, $\frac{1}{2}^-$; 3.09 MeV, $\frac{1}{2}^+$; 3.68 MeV, $\frac{3}{2}^-$; 3.85 MeV, $\frac{5}{2}^+$. The next states are about 7 MeV and above. Interpret these four states according to the shell model.
3. The level scheme of Figure 5.6 would lead us to expect $I^\pi = \frac{11}{2}^-$ for the ground state of ^{203}Tl ($Z = 81$), while the observed value is $\frac{1}{2}^+$. A similar case occurs in ^{207}Pb ($N = 125$) and ^{199}Hg ($N = 119$), where $\frac{13}{2}^+$ is expected but $\frac{1}{2}^-$ is observed. Given that the pairing force increases strongly with ℓ , give the shell-model configurations for these nuclei that are consistent with the observed spin-parity assignments.
4. Figure 5.6 is only a schematic, average representation of the shell-model single-particle states. The energies of the states will vary with the proton number and neutron number. To illustrate this effect, consider the available states of the 51st proton in Sb isotopes. Make a chart in the style of Figure 5.25 showing the $\frac{5}{2}^+$ and $\frac{7}{2}^+$ states in ^{113}Sb to ^{133}Sb . (Consult the *Table of Isotopes* and the Nuclear Data Sheets for information on the energy levels.) Discuss the relative positions of the $g_{7/2}$ and $d_{5/2}$ proton states as a function of neutron number.
5. In the single-particle shell model, the ground state of a nucleus with an odd proton and an odd neutron is determined from the coupling of the proton and neutron shell-model states: $I = j_p + j_n$. Consider the following nuclei: $^{16}\text{N} - 2^-$; $^{12}\text{B} - 1^+$; $^{34}\text{P} - 1^+$; $^{28}\text{Al} - 3^+$. Draw simple vector diagrams illustrating these couplings, then replace j_p and j_n , respectively, by $\ell_p + s_p$ and $\ell_n + s_n$. Examine your four diagrams and deduce an empirical rule for the relative orientation of s_p and s_n in the ground state. Finally, use your empirical rule to predict the I^π assignments of ^{26}Na and ^{28}Na .
6. (a) If the energy of a single-particle state in the absence of spin-orbit splitting is E_0 , find the energies of the two members of the spin-orbit doublet whose difference is given by Equation 5.4. (b) Show that the “center of gravity” of the doublet is E_0 .
7. Compute the expected shell-model quadrupole moment of ^{209}Bi ($\frac{9}{2}^-$) and compare with the experimental value, -0.37 b.
8. Compute the values of the magnetic dipole moments expected from the shell model, and compare with the experimental values:

Nuclide	I^π	$\mu(\text{exp}) (\mu_N)$
^{75}Ge	$\frac{1}{2}^-$	+0.510
^{87}Sr	$\frac{9}{2}^+$	-1.093
^{91}Zr	$\frac{5}{2}^+$	-1.304
^{47}Sc	$\frac{7}{2}^-$	+5.34
^{147}Eu	$\frac{11}{2}^-$	+6.06

9. Compute the vibrational frequency associated with typical quadrupole vibrations. Taking typical values for decay lifetimes of 2^+ states in vibrational nuclei (you can find these in the *Table of Isotopes*, for example), comment on whether the decays generally occur on a shorter or longer time scale than the nuclear vibrations. If α represents the vibrational amplitude, as in Equation 5.13, could we observe quantities dependent on $\langle\alpha\rangle$? On $\langle\alpha^2\rangle$?
10. By tabulating the possible m states of three quadrupole ($\ell = 2$) phonons, and their symmetrized combinations, show that the permitted resultant states are 0^+ , 2^+ , 3^+ , 4^+ , and 6^+ .
11. Find the volume of the nucleus whose surface is described by Equation 5.14.
12. Consider a uniformly charged ellipsoidal nucleus whose surface is described by Equation 5.14. Show that the electric quadrupole moment, defined by Equation 3.36, is given by Equation 5.16.
13. The levels of ^{174}Hf show two similar rotational bands, with energies given as follows (in MeV):

	$E(0^+)$	$E(2^+)$	$E(4^+)$	$E(6^+)$	$E(8^+)$	$E(10^+)$	$E(12^+)$
Band 1	0	0.091	0.297	0.608	1.010	1.486	2.021
Band 2	0.827	0.900	1.063	1.307	1.630	2.026	2.489

Compare the moments of inertia of these two bands, and comment on any difference.

14. The low-lying levels of ^{17}O and ^{19}O differ primarily in the presence of states of $I^\pi = \frac{3}{2}^+$ and $\frac{9}{2}^+$ in ^{19}O ; these two states have no counterparts in ^{17}O . Show that these two states could result from the configuration $(d_{5/2})^3$ and thus are not expected in ^{17}O .
15. The nucleus ^{24}Mg has a 2^+ first excited state at 1.369 MeV and a 4^+ second excited state at 4.123 MeV. The 2^+ state has a magnetic dipole moment of $1.02 \mu_N$ and an electric quadrupole moment of -0.27 b . Which model would be most likely to provide an accurate description of these states? Justify your choice by calculating parameters appropriate to your choice of model.

UNIT II NUCLEAR DECAY AND RADIOACTIVITY